HHS Public Access

Author manuscript

Sci Signal. Author manuscript; available in PMC 2020 October 19.

Published in final edited form as:

Sci Signal. ; 13(646): . doi:10.1126/scisignal.aba3043.

An allosteric site on MKP5 reveals a strategy for small molecule inhibition

Zachary T. K. Gannam[1,10], **Kisuk Min**[1,11], **Shanelle R. Shillingford**[1,2], **Lei Zhang**[1], **James Herrington**[3], **Laura Abriola**[3], **Peter C. Gareiss**[3], **Georgios Pantouris**[1,12], **Argyrios Tzouvelekis**[4], **Naftali Kaminski**[5], **Xinbo Zhang**[6], **Jun Yu**[7], **Haya Jamali**[2], **Jonathan A. Ellman**[2], **Elias Lolis**[1,*], **Karen S. Anderson**[1,8,*], **Anton M. Bennett**[1,9,*]

[1]Department of Pharmacology, Yale University School of Medicine, New Haven, CT 06520, USA

[2]Department of Chemistry, Yale University, New Haven, CT 06511, USA

[3]Yale Center for Molecular Discovery, Yale West Campus, West Haven, CT 06516, USA

[4]"Alexander Fleming" Biomedical Sciences Research Center, 16672, Vari, Greece

[5]Department of Internal Medicine, Section of Pulmonary, Critical Care and Sleep Medicine, Yale University School of Medicine, New Haven, CT 06520, USA

[6]Department of Internal Medicine, Temple University Lewis Katz School of Medicine, Philadelphia, PA 19140, USA

[7]Center for Metabolic Disease Research and Department of Physiology, Temple University Lewis Katz School of Medicine, Philadelphia, PA 19140, USA

[8]Department of Molecular Biophysics and Biochemistry, New Haven, Connecticut 06520, USA

[9]Program in Integrative Cell Signaling and Neurobiology of Metabolism, Department of Comparative Medicine, Yale University School of Medicine, New Haven, CT 06520, USA

[10]Current address: Department of Biology, Washington University, St. Louis, MO 63130

[11]Current address: Department of Kinesiology, University of Texas, El Paso, TX 79968

[12]Current address: Department of Chemistry, University of the Pacific, Stockton, CA 95211

Abstract

[*]To whom correspondence should be addressed. Anton M. Bennett, Ph.D., Yale University School of Medicine, Department of Pharmacology, SHM B226D, 333 Cedar Street, New Haven, CT 06520-8066, USA. anton.bennett@yale.edu; Elias Lolis, Ph.D., elias.lolis@yale.edu; Karen Anderson, Ph.D., karen.anderson@yale.edu.

Author contributions: P.C.G., J.H., L.A., L.Z. and A.M.B. designed and carried out high-throughput screen. Cloning, protein expression and protein purification were conducted by Z.T.K.G., S.R.S., L.Z. and G.P. Z.T.K.G., S.R.S, L.A. and J.H. performed *in vitro* experiments. Z.T.K.G. carried out crystallography and modelling. S.R.S., K.M., and L.Z. performed cellular assays and K.M. conducted animal studies. H.J. and J.A.E. designed and carried out synthesis of Compound 1. A.T., N.K., X.Z. and J.Y. advised on the TGF-β1 experiments. K.S.A., A.M.B., and E.L. advised on experiments and interpretation of results. Z.T.K.G. and A.M.B. drafted this manuscript, which was then edited by Z.T.K.G., E.L., K.S.A., and A.M.B.

Competing interests: The authors declare that they have no competing interests.

Data availability: Atomic coordinates and structure factors for MKP5-CD:Compound 1 have been deposited at the Protein Data Bank under the accession code 6MC1. All other data needed to evaluate the conclusions in the paper are present in the main paper or the Supplementary Materials. Compound 1 requires a material transfer agreement from Yale University.

The mitogen-activated protein kinase (MAPK) phosphatases (MKPs) have been considered “undruggable”, but their position as regulators of the MAPKs makes them promising therapeutic targets. MKP5 has been suggested as a potential target for the treatment of dystrophic muscle disease. Here, we identified an inhibitor of MKP5 using a p38α MAPK-derived phosphopeptide-based small molecule screen. We solved the structure of MKP5 in complex with this inhibitor, which revealed an undescribed allosteric binding pocket. Binding of inhibitor to this pocket collapsed the MKP5 active site and was predicted to limit MAPK binding. Treatment with the inhibitor recapitulated the phenotype of MKP5 deficiency resulting in activation of p38 MAPK and JNK. We demonstrated that MKP5 was required for TGF-β1 signaling in muscle and that the inhibitor blocked TGF-β1–mediated Smad2 phosphorylation. TGF-β1 pathway antagonism has been proposed for the treatment of dystrophic muscle disease. Thus, allosteric MKP5 inhibition represents a therapeutic strategy against dystrophic muscle disease.

Editor’s Summary:

Drugging an “undruggable” phosphatase

The MAPK family of kinases regulate diverse physiological and pathophysiological processes and are inactivated by MAPK phosphatases including MKP5. Blocking MKP5 activity has emerged as a potential treatment for dystrophic muscle disease. Gannam *et al.* identified and characterized a small molecule that inhibited MKP5 by binding to an allosteric site on the phosphatase, but that did not affect the activity of other related phosphatases. In muscle cells, the inhibitor blocked MKP5 from inactivating the MAPKs and inhibited the TGF-β signaling pathway that results in fibrosis in dystrophic muscle disease. These results demonstrate that it is possible to allosterically target MAPK phosphatases with a high degree of specificity, opening avenues for the treatment of diseases for which MAPK phosphatase inhibition confers therapeutic benefit.

One-Sentence Summary:

A small molecule inhibitor of the phosphatase MKP5 identifies an allosteric site that enables specific targeting.

INTRODUCTION

Protein phosphorylation is a critical post-translational modification controlled by the actions of both protein kinases and protein phosphatases. The mitogen-activated protein kinases (MAPKs) are a family of serine/threonine kinases that play indispensable roles in signal transduction pathways that control a plethora of physiological responses (1). Dysregulation of MAPK activity is causal to the pathogenesis of many human diseases, including cancer, obesity and diabetes, and diseases of the immune, cardiac and musculoskeletal systems (2–6). Therefore, exquisite regulation of this activity is crucial to maintaining health. One major regulator of the MAPKs is the family of MAPK phosphatases (MKPs), a subset of the dual-specificity phosphatases (DUSPs) (7). By directly dephosphorylating the regulatory tyrosine and threonine residues on the activation loop of MAPKs, the MKPs can inactivate these kinases (8). Although MKPs share a common fold with the DUSPs and the larger family of protein tyrosine phosphatases (PTPs), they have a kinase interaction motif (KIM) distal to the catalytic domain that allows them to bind directly and discriminate amongst MAPK

substrates, often triggering a conformational shift in the catalytic domain to facilitate dephosphorylation (9, 10). The MKPs are divided into three subfamilies based on their MAPK substrate selectivity and subcellular localization, with one group including MKP5, MKP7, and DUSP8 that specifically dephosphorylates the stress-activated MAPKs, p38 MAPK and c-Jun NH_2-terminal kinase (JNK). These mechanisms allow the MKPs to exhibit tight control over MAPK activity (7).

The MKPs have emerged with roles in many disorders, including diseases of the immune (11) and cardiovascular systems (12), cancer (13), malaria (14), metabolic syndrome (15, 16), and dystrophic muscle diseases (17, 18). Previously, we have shown that MKP5 is a potential target for the treatment of dystrophic muscle disease (18). Specifically, Duchenne muscular dystrophy (DMD) is an inevitably fatal X-linked genetic disorder caused by a loss-of-function mutation in dystrophin, which renders the myofiber highly susceptible to injury (19). When skeletal muscle is unable to regenerate, as is the case in DMD, the damaged muscle is eventually replaced with fibrotic tissue (20, 21). Development of fibrosis is at least partially mediated by the transforming growth factor β1 (TGF-β1) signaling pathway, the modulation of which is a potential strategy to treat dystrophic muscle disease (22–24). Cumulative acquisition of fibrotic skeletal muscle results in reduced skeletal muscle strength and impaired mobility followed by early death often due to cardio-respiratory complications. Although there have been developments in the field of DMD treatments, there is still an unmet need for therapeutics. Mice lacking the expression of MKP5 exhibit enhanced regenerative myogenesis (18). Further, genetic ablation of MKP5 in the context of a mouse model of DMD ameliorates the dystrophic muscle phenotype (18). These results suggest a role for MKP5 in the progression of DMD and demonstrate the potential utility of an MKP5 inhibitor for the treatment of DMD and potentially other dystrophic muscle diseases.

Although MKP5 and other MKPs are tempting targets for the treatment of many diseases, the PTPs and DUSPs have long been considered “undruggable” (25). The catalytic pocket of these protein phosphatases is well conserved, making specific inhibition difficult (25). Further, the catalytic pocket is positively charged, such that complementary compounds are frequently negatively charged and often suffer from poor bioavailability. Although targeting the catalytic pocket of PTPs and DUSPs has been a largely ineffective endeavor, there has been a resurgence in interest in these proteins as targets for allosteric modulation of catalytic activity. Allosteric inhibitors of the PTPs SHP2 and PTP1B have been identified, with the former arising from a high-throughput screening specifically optimized to identify allosteric modulators (26, 27). Identification of allosteric sites and small molecules binding these regions has renewed interest in strategies for therapeutics targeting PTPs and DUSPs for a wide array of diseases.

In the interest of targeting MKP5 to treat dystrophic muscle disease, we described in this study a small molecule inhibitor of MKP5 identified by a high-throughput MAPK phosphopeptide-based screen. By co-crystallizing MKP5 with this inhibitor, we solved the structure of an MKP in complex with a small molecule inhibitor, which showed that the compound bound to MKP5 at a previously undescribed allosteric site. We showed that MKP5 was required for the activation of the TGF-β1 pathway. The levels of TGF-β1 are increased in muscular dystrophy, which causes fibrosis and impairs skeletal muscle function,

making this pathway a therapeutic target for this disease (22–24, 28). Skeletal muscle of MKP5-deficient mice and fibroblasts exhibited reduced Smad2 activity and the MKP5 inhibitor attenuated TGF-β1-mediated Smad2 phosphorylation in fibroblasts. The compound and allosteric site on MKP5 are the initial steps toward the development of a highly specific, potent, orally bioavailable MKP5 inhibitor. Our results suggest that such an inhibitor represents a strategy for the treatment of dystrophic muscle disease for which to-date there is neither an effective treatment nor cure.

RESULTS

A high-throughput screen identifies an inhibitor of MKP5

We previously found that when MKP5-deficient mice were intercrossed with a mouse model of Duchenne muscular dystrophy (*mdx*), these mice were protected from the development of dystrophic muscle disease accompanied by a marked reduction in skeletal muscle fibrosis (18). These results imply that inactivation of MKP5 could serve as a therapeutic strategy for the treatment of dystrophic muscle disease. Thus, we set out to identify potential MKP5 inhibitors. Previous efforts to identify inhibitors of PTPs and DUSPs have utilized small molecule mimics of phosphotyrosine such as *para*-nitrophenyl phosphate (*p*NPP) as substrates (29). In order to increase the likelihood of identifying compounds that bind at sites distinct from the MKP5 catalytic pocket, we chose to use a modified 11 amino acid dually-phosphorylated peptide (Asp-Asp-Glu-Nle-pThr-Gly-pTyr-Val-Ala-Thr-Arg) encompassing the $pThr^{180}$-Gly-$pTyr^{182}$ motif present on the activation loop of p38α MAPK, which represents the physiological MKP5 substrate (30). An optimized high-throughput malachite green phosphatase assay was developed. We screened 162,154 compounds from commercial and proprietary libraries for the inhibition of phosphatase activity of the catalytic domain of MKP5 (MKP5-CD, residues 320-467) against the p38α MAPK phosphopeptide substrate (Fig. 1A). The resultant screen yielded a Z' value of 0.7-0.8 (fig. S1) and identified 391 compounds that inhibited MKP5-CD by more than 30% (Fig. 1B).

The 391 compounds were re-tested, analyzed for assay interference and checked for historical promiscuity in high throughput screens. Following this triage, 27 compounds were assayed for selectivity for DUSPs as compared with PTPs. The compounds were tested for inhibition of the 46 kDa isoform of the striatal-enriched PTP (STEP-46) and PTP-1B. We determined that 3,3-dimethyl-1-((9-(methylthio)-5,6-dihydrothieno[3,4-*h*]quinazolin-2-yl)thio)butan-2-one (Compound 1, Fig. 1C), displayed differential activity between MKP5-CD (half-maximal inhibitory concentration, IC_{50} ~ 3.9 μM), STEP-46 (IC_{50} > 200 μM), and PTP-1B (IC_{50} > 100 μM) (fig. S2). As such, Compound 1 was designated as our lead hit. The core three-ring structure of Compound 1 is rare and represents a novel chemical scaffold. In order to carry out all further studies, Compound 1 was re-synthesized according to the scheme in fig. S3.

To further characterize Compound 1, we carried out a microscale thermophoresis assay using MKP5-CD to determine the binding affinity of Compound 1 for MKP5. We found that Compound 1 bound to fluorescently-labeled MKP5-CD with a dissociation constant (K_d) of 1.0 ± 0.2 μM (Fig. 1D). The potency of Compound 1 was determined by malachite green assay using the p38α MAPK phosphopeptide as a substrate, which indicated an IC_{50} of 3.9

± 0.6 μM (Fig. 1E). Compound 1 notably did not fully inhibit the phosphatase activity of MKP5-CD, likely due to its modest solubility (Supplementary Materials). Compound 1 also inhibited the full-length MKP5 with similar potency to the catalytic domain (fig. S4). In order to demonstrate the selectivity of Compound 1, we tested its ability to inhibit other members of the MKP family, MKP1, MKP3, and MKP7. All three phosphatases were substantially resistant to inhibition by Compound 1, with all showing an increase in IC_{50} of at least 16-fold (Fig. 1E–F). Together, these results identify Compound 1 as a selective inhibitor of MKP5.

To determine the mode of inhibition of Compound 1 against MKP5, we optimized a kinetic assay based on the fluorescence of tagged phosphate-sensing protein using purified recombinant full-length dually-phosphorylated p38α MAPK as a substrate. This assay revealed a K_m of 27.5 ± 3.1 μM and a k_{cat} of 0.62 ± 0.02 s^{-1} using purified recombinant full-length dually-phosphorylated p38α MAPK as a substrate (table S1). The p38α MAPK phosphopeptide was not conducive to this analysis due to its high K_m (table S1). By measuring the initial velocities of phosphatase activity of MKP5-CD in the presence of varying concentrations of both Compound 1 and p38α MAPK, we were able to determine the effect of Compound 1 on the mechanism of catalysis. When these data were fit to a mixed-mechanism inhibition curve (31), we found that Compound 1 displayed a mixed competitive mode of inhibition ($\alpha \approx 17.4$) with a K_i of 8.9 ± 2.2 μM (Fig. 1G, fig. S5). There was a significant effect on the apparent K_m, which shifts from 25 ± 3.5 μM in the absence of Compound 1 to 51 ± 7.8 μM in the presence of 10 μM Compound 1 (table S2). Additionally, when using Compound 1 against p38α MAPK as substrate, the apparent IC_{50} of Compound 1 increased linearly with increasing concentration of p38α MAPK (table S2). These results suggest a substantial competitive nature of the inhibition by Compound 1 using p38α MAPK as a substrate. To investigate further the mechanism of inhibition of Compound 1 we assessed the effects of a small molecule phosphomimetic which directly interacts with the active site. Although *p*NPP has typically been used as a small molecule phosphomimetic for the analysis phosphatase catalytic mechanisms the reported K_m for MKP5-CD against *p*NPP of 36 mM (46) was prohibitive. Instead, the small molecule phosphatase substrate 6,8-difluoro-4-methylumbelliferyl phosphate (DiFMUP) was found to be a suitable alternative exhibiting a K_m of 71.8 ± 5.8 μM (table S1). Using DiFMUP as substrate we obtained similar results that again demonstrated a mixed mechanism of inhibition ($\alpha = 4.2$) (fig. S6, A to C and table S3) accompanied by a decrease in K_m from 70 μM in the absence of Compound 1 to 124 μM in the presence of 50 μM of Compound 1 (table S3). A similar linear increase in IC_{50} of Compound 1 was observed with increasing DiFMUP (table S3). Thus, when DiFMUP is used as substrate Compound 1 exerts a lower α value indicating a less competitive nature for the mode of inhibition.

Finally, in order to examine the effect of Compound 1 on MKP5 catalysis, a transient kinetics methodology using stopped-flow fluorescence was employed. First, we demonstrated that MKP5-CD displays a biphasic burst of product formation when dephosphorylating DiFMUP, implying that product release was rate-limiting (fig. S7, A and B). However, in the presence of 20 and 40 μM Compound 1, the burst rate (k_1) decreased from 8.4 ± 0.2 s^{-1} to 1.2 ± 0.02 s^{-1}, a 7-fold change (Fig. 1H). These data demonstrate that Compound 1 inhibits MKP5 activity by directly slowing the rate of chemical catalysis. In

addition, in the presence of inhibitor there is no longer biphasic formation. Instead, the linear formation of product indicates that the rate-limiting step has shifted from product release to chemical catalysis when Compound 1 is bound in the allosteric site.

The crystal structure of MKP5-CD in complex with Compound 1 identifies an allosteric site

The *apo* structure of MKP5-CD has been solved previously (32, 33). Therefore, to further shed light on the mechanism of inhibition of Compound 1, crystals of the MKP5-CD-Compound 1 complex were grown and the structure of MKP5-CD bound to Compound 1 was solved at 2.7 Å resolution with an R_{free} of 0.227 (table S4, fig. S8). The asymmetric unit contains six monomers with nearly identical conformations. Electron density for the inhibitor molecule was well-defined and found in all six polypeptide chains (Fig. 2A). We found that Compound 1 bound to an allosteric site formed by the alpha helices α3, α4, and α5, as well as the α4-α5 loop (Fig. 2B). This pocket, located approximately 8 Å from the catalytic sulfhydryl of Cys^{408}, has not previously been described, though residues on helices α4 and α5 have been identified as important for JNK binding (9). Key interactions between Compound 1 and MKP5 include a parallel-displaced π-stacking interaction with Tyr^{435} and a hydrogen bond with the backbone amide of Asn^{448} (Fig. 2C). The compound also makes extensive hydrophobic interactions with many residues, including Tyr^{435}, Pro^{447}, and Met^{452}. Despite binding to an allosteric site, Compound 1 forms a hydrophobic interaction with Ser^{413} of the β5-α3 loop, which forms part of the catalytic pocket.

In the highest-resolution crystal structure of *apo*-MKP5-CD available, two polypeptide chains adopt similar, but not identical conformations (32). The first chain is described as taking an active conformation similar to that seen in other DUSPs. There are multiple differences between the structure of the MKP5-CD-Compound 1 complex and the *apo* active conformation (Fig. 3A). The most striking of these differences is the movement of the residues $^{445}ISP^{447}$ in the α4-α5 loop, where the peptide backbone shifts 3.7 Å to accommodate the incoming inhibitor. As part of this movement, the sidechain of Pro^{447} flips out of the pocket, moving ~6.5 Å. Other residues in the allosteric site move to better interact with Compound 1, including Tyr^{435}, which rotates and shifts to allow its ring-stacking interaction with the compound. The shift in the α4-α5 loop forces the β5-α3 loop, which forms the catalytic site, to compensate and change conformation as well. Although the positions of the catalytic residues Cys^{408}, Asp^{377}, and Arg^{414} are not substantially affected, there is a major reorganization in the backbone leading to the displacement of residues $^{410}AGVS^{413}$. As a result of this shift in conformation, the volume of the active site pocket decreases in a statistically significant manner by nearly 18% (Fig. 3B–C, table S5). These residues are also responsible for coordinating the phosphate group of the incoming phosphotyrosine or phosphothreonine by a series of hydrogen bonds with the peptide backbone (34). The deformation of the β5-α3 loop prevents the formation of most of these hydrogen bonds, limiting proper orientation of the substrate in the active site pocket. Previously performed molecular dynamics simulations of MKP5-CD indicate that these shifts are unlikely to occur in solution in the absence of inhibitor (35).

Residues in the allosteric pocket govern Compound 1 inhibition and MKP5 selectivity

The PTP domains in other DUSPs are between 36 and 57% identical to that of MKP5, with those in the other stress-activated MAPK-specific MKPs (MKP7 and DUSP8) displaying the highest degree of similarity. Many of the residues in MKP5 that interact with Compound 1 are well-conserved through the DUSPs, with 8 of 10 residues bearing considerable similarity, including Tyr^{435}. An aromatic residue is nearly always found at this position within the α4 helix, suggesting that this residue might play an important role in either MKP5 enzymatic activity and/or inhibitor binding. To investigate the importance of the allosteric pocket for the specific inhibition of MKP5, we generated mutants of Tyr^{435}, a potential key residue that contributes to the binding of Compound 1 and characterized their enzymatic activity and capacity for inhibition by Compound 1. Tyr^{435} is well-conserved as an aromatic residue in nearly all DUSPs (Fig. 4A) and as indicated contributes to a π-stacking interaction with Compound 1. We replaced Tyr^{435} with either alanine, serine, or tryptophan. Although all three mutant constructs folded properly (fig. S9), only the Y435W mutant maintained substantial activity against either *p*NPP (Fig. 4B) or p38α MAPK phosphopeptide (fig. S10). In addition, binding and inhibition experiments demonstrated that Compound 1 was capable of binding to and inhibiting the activity of only the Y435W mutant (Fig. 4C, fig. S11, A and B). These data identify Tyr^{435} as essential for phosphatase activity and Compound 1 binding.

Although our data demonstrating substantially reduced potency of Compound 1 between MKP5 and other MKPs suggest that Compound 1 could attain selectivity amongst the MKPs, it was unlikely that this selectivity is due to Tyr^{435} because this residue is conserved among the MKPs (Fig. 4A). However, we noted that the allosteric pocket of MKP5 contains the residues Met^{431} and Thr^{432}, which do not exist within the allosteric pocket of either MKP1 or MKP7. Therefore, we mutated Met^{431} and Thr^{432} in MKP5 to the corresponding residues in MKP1 and MKP7, Leu^{431} and Asp^{432}, respectively. The catalytic activity of the MKP5 single mutants M431L, T432D and double mutant M431L/T432D were comparable to wild type MKP5 when measured against either *p*NPP (Fig. 4B) or p38α MAPK phosphopeptide (fig. S10). The MKP5 single mutants M431L and T432D exhibited IC_{50} values for inhibition of MKP5 that were markedly increased to 99 and 61 μM, respectively. The M431L/T432D double mutation nearly abolished inhibition of MKP5 by Compound 1 (Fig. 4C, fig. S12, A and B). Concomitant reductions in the binding affinity for these mutants were observed. These data demonstrate that the allosteric pocket of MKP5 is further defined by residues Met^{431} and Thr^{432} and that Compound 1 acquires selectivity for MKP5 over the other MKPs through these residues.

Compound 1 inhibition of MKP5 induces MAPK activity and stimulates myoblast differentiation

After demonstrating the efficacy of Compound 1 *in vitro*, we next sought to determine whether Compound 1 exhibited cell-based activity towards MKP5. MKP5 primarily dephosphorylates p38α MAPK and JNK but demonstrates little to no activity against extracellular signal-regulated kinases 1 and 2 (ERK1/2) (30). Consistent with this selectivity, myoblasts isolated from MKP5-deficient mice exhibit approximately 2-3-fold increases in p38α MAPK and JNK phosphorylation, but no change in ERK1/2 activation (18). We first

sought to measure the activation of these MAPKs upon treatment with Compound 1 in cellular studies. In C2C12 mouse myoblasts treated with Compound 1, we found that the activation of p38α MAPK was increased in a dose-dependent manner by up to 4-fold at the highest concentration of Compound 1 (Fig. 5A). JNK activation was also increased up to 2-fold at the highest concentration of Compound 1 upon treatment of C2C12 myoblasts (Fig. 5A). In contrast, Compound 1 did not alter the activation of ERK1/2 even at the highest concentration of Compound 1 (Fig. 5A). These results demonstrate that Compound 1 selectively enhances p38α MAPK and JNK activities in a cellular context. Moreover, a lack of ERK1/2 activation with Compound 1 implies that the compound does not exert broad non-specific inhibition amongst other MKPs. Compound 1 did not affect C2C12 myoblast proliferation (Fig. 5B). However, when C2C12 myoblasts were initiated to undergo differentiation and treated with Compound 1 for 72 h, myoblast differentiation was significantly increased as determined by quantifying the myotube fusion index (Fig. 5C). The increase in myoblast differentiation by Compound 1 recapitulated the effects previously observed in primary myoblasts isolated from *Mkp5*$^{-/-}$ mice (18). These data demonstrate that treatment of C2C12 myoblasts with Compound 1 phenocopies myoblasts derived from MKP5-deficient mice, likely by selectively enhancing the activity of p38α MAPK and/or JNK.

MKP5 is required for TGF-β1 signaling and Compound 1 inhibits Smad2 activity

In light of our previous observations that MKP5 may serve as a target for the treatment of dystrophic muscle disease, we sought to identify a mechanism through which MKP5 inhibition might ameliorate the disease. Mice lacking MKP5 expression on the *mdx* background are protected from the development of skeletal muscle fibrosis (18). We hypothesized that MKP5 might be involved in the progression of fibrosis, which is driven by the TGF-β1 signaling pathway (23, 24, 28). Disruption of TGF-β1 activity in *mdx* mice curtails fibrosis and subsequently improves the dystrophic phenotype (36). In response to injury the expression levels of TGF-β1 increases resulting in activation of the transcription factor Smad2 by phosphorylation, leading to nuclear translocation and induction of fibrogenic genes (22, 36, 37). We determined the effects on Smad2 phosphorylation in mice lacking expression of MKP5 (*Mkp5*$^{-/-}$) in response to injury using cardiotoxin injection into skeletal muscles. We found that Smad2 phosphorylation was significantly reduced in *Mkp5*$^{-/-}$ mice at 4 and 10 days following cardiotoxin-induced muscle injury as compared with wild type mice (Fig. 6A). These results demonstrate that MKP5 is involved in promoting Smad2 activity in skeletal muscle of mice.

Next, mouse embryonic fibroblasts (MEFs) isolated from *Mkp5*$^{+/+}$ and *Mkp5*$^{-/-}$ mice were treated with TGF-β1 and the effects on Smad2 phosphorylation assessed. We found that Smad2 phosphorylation was significantly inhibited in TGF-β1-treated *Mkp5*$^{-/-}$ MEFs as compared with *Mkp5*$^{+/+}$ MEFs (Fig. 6B). When MEFs derived from *Mkp5*$^{+/+}$ mice were treated with Compound 1, we found that the compound inhibited TGF-β1-mediated Smad2 phosphorylation (Fig. 6B). Concomitantly, Compound 1 treatment resulted in a dose-dependent increase in the phosphorylation of both p38α MAPK and JNK, but not of ERK1/2 in wild type MEFs (Fig. 6B). In order to substantiate the interpretation that Compound 1 acted through MKP5 to inhibit Smad2 phosphorylation, we sought to

determine the ability of Compound 1 to perturb TGF-β1-mediated Smad2 phosphorylation in *Mkp5*$^{-/-}$ MEFs. Smad2 phosphorylation was inhibited in TGF-β1 stimulated *Mkp5*$^{-/-}$ MEFs as compared with *Mkp5*$^{+/+}$ MEFs and Compound 1 failed to inhibit Smad2 phosphorylation further in *Mkp5*$^{-/-}$ MEFs (Fig. 6C). Moreover, the phosphorylation of p38α MAPK and JNK was enhanced in *Mkp5*$^{-/-}$ MEFs but treatment with Compound 1 did not result in additional phosphorylation of these MAPKs. Notably, ERK1/2 was unaffected in either *Mkp5*$^{-/-}$ MEFs or in *Mkp5*$^{-/-}$ MEFs treated with Compound 1 (Fig. 6C). Collectively, these data argue that MKP5 inhibition by Compound 1 attenuates TGF-β1-signaling and provides a mechanistic explanation for how MKP5 targeting may serve as a therapeutic pathway for the treatment of dystrophic muscle disease.

DISCUSSION

The role MKP5 plays in the progression of dystrophic muscle disease prompted us to conduct a high-throughput screen to identify potential inhibitors of the phosphatase. Recognizing that PTPs and DUSPs present a considerable challenge as drug targets, largely due to the high degree of conservation and positive charges in their catalytic site, we increased the possibility of identifying non-catalytic site-directed inhibitors by using a dually-phosphorylated peptide representing the primary substrate of MKP5, p38α MAPK. The high-throughput screen against the catalytic domain of MKP5 identified a unique inhibitor with low micromolar potency. We obtained the structure of MKP5 in complex with a small molecule inhibitor through co-crystallography. These studies revealed an allosteric binding site occupied by the inhibitor, the binding of which caused a partial collapse of the catalytic pocket, which may prevent access of the substrate to the catalytic sulfhydryl. These structural studies are supported by our transient kinetic analysis of the catalytic mechanism. This analysis showed a biphasic burst of product formation with the rate of the faster phase reflecting chemical catalysis at 8.4 s^{-1} and defining the overall rate-limiting step in enzyme catalysis as product release. In the presence of the inhibitor, a burst of product is absent and replaced by a linear formation of product revealing a shift in the overall rate-limiting step from product release to chemical catalysis at a reduced rate of 1.2 s^{-1}. Thus, the inhibitor slows the kinetic reaction pathway from product release to the chemical catalysis step. Treatment of myoblasts with the inhibitor resulted in the selective activation of both p38α MAPK and JNK, but not ERK, as well as enhancement of myoblast differentiation, features that were recapitulated in MKP5-deficient myoblasts. Finally, we uncovered a relationship between MKP5 and the TGF-β1 pathway, which has been implicated in the development of fibrosis in dystrophic muscle disease. We demonstrated that MKP5 was required for TGF-β1 signaling, which was blocked by the inhibitor. These results reveal an unanticipated approach to target MKP5 by small molecules and suggests a potential mechanism of action through which MKP5 antagonism might serve as a therapeutic strategy for the treatment of dystrophic muscle disease.

We used steady-state kinetic analysis to determine the pattern of inhibition of MKP5 by Compound 1. A kinetic characterization of MKP5 activity against either p38α MAPK or DiFMUP in the presence of Compound 1 indicated a mixed mode of inhibition, whereby both substrate affinity and maximal reaction velocity were decreased (that is, both competitive and noncompetitive inhibition are observed). Although it is uncommon for

inhibitors binding allosteric sites to compete with substrate, this phenomenon has been previously reported (38–40). The noncompetitive component of this mechanism was likely a result of the partial collapse of the active site highlighted by our structural studies. This was corroborated by our transient kinetic analysis with DiFMUP, which showed that the rate of chemistry is significantly slowed by Compound 1. The partially competitive component of the inhibition may be understood by comparing our structure to previously published structures of DUSP catalytic domains bound to substrates. Of particular interest is the complex between MKP7-CD and JNK1, which unlike most DUSP-kinase complexes, is formed entirely by interactions within the MKP7 catalytic domain (41). Models of MKP5-CD in complex with either JNK1 or p38α MAPK (42) (Fig. 7A and fig. S13, respectively) show a substantial clash between the C-lobes of both kinases and Compound 1. Specifically, residues in JNK (^{229}DHI^{231}) critical for MKP5 binding (41) are predicted to clash with Compound 1. Further, we overlaid MKP5-CD with the structure of human vaccinia H1-related phosphatase (VHR) in complex with a phosphopeptide similar to that used in our activity assays (43) (Fig. 7B). This model suggests that the α4-α5 and β5-α3 loops of MKP5, which both shift upon Compound 1 binding, will clash with the substrate activation loop. Residues in the phosphopeptide corresponding to ^{182}YVAT^{185} in p38α MAPK are predicted to clash with the reorganized MKP5 loops.

The collapse of the active site and the direct and indirect clashes with substrate suggested above are summarized as a three-pronged mechanism of inhibition in Fig. 7C. We propose that formation of the enzyme-substrate-inhibitor complex is hindered, and that conformational shifts and steric interference prevent the phosphotyrosine and phosphothreonine of substrate MAPK from adopting an optimal position in relation to the catalytic residues of MKP5. It is likely because of this multi-faceted mechanism of inhibition that the relative strength of competitive and noncompetitive inhibition varies between small molecule substrates and full-length p38α MAPK. Because small molecule substrates like *p*NPP and DiFMUP interact with MKP5 only at the active site, they are not subject to clashes with the compound itself, and thus encounter more noncompetitive inhibition (fig. S6, table S3). Conversely, p38α MAPK engages with all three mechanisms of inhibition and is subject to more competitive inhibition (Fig. 1G, Fig. S5, table S2). Further, as MKP5 binds p38α MAPK and JNK through substantially different interactions, it is likely that Compound 1 differentially inhibits the dephosphorylation of each (9, 41). This may explain the apparent difference in activation of p38 MAPK and JNK in our cellular studies (Fig. 5A and 6B).

The allosteric pocket bound by Compound 1 has not been previously observed although some residues in the alpha helices α4 and α5 as well as the α4-α5 loop that comprise the allosteric site are involved with JNK binding (41). Further, NMR studies have suggested that regions in VHR corresponding to the α5 helix and Met^{452} may be targets for the allosteric inhibition of that phosphatase (44). The residues Met^{431}, Thr^{432}, and Met^{452}, all of which form hydrophobic interactions with Compound 1 and display slight shifts upon inhibitor binding, have been proposed to interact with JNK. The JNK residues Asp^{229} and Ile^{231} to a lesser extent are essential for formation of the MKP5-JNK complex. Our molecular models predict that those residues would clash directly with Compound 1 bound in the allosteric pocket. In addition, our mutational analysis validated that Met^{431}, Thr^{432}, and Tyr^{435} are

critical for inhibition by Compound 1 and, in the case of the latter, catalytic activity. This work serves to support the notion that the allosteric pocket plays an important role in MAPK interaction and MKP activity.

Development of PTP inhibitors has long been curtailed by poor selectivity. However, we showed that Compound 1 inhibited other MKPs (such as MKP1, MKP3, and MKP7) with at least 16-fold reduced potency than MKP5. These results indicate that the allosteric pocket of MKP5 contains determinants of specificity (Met^{431} and Thr^{432}) and thus, selectivity amongst the MKPs that can be exploited by targeting this region. In this regard, our cell-based assays demonstrated that Compound 1 preferentially activated p38α MAPK and JNK over that of ERK1/2. These results are consistent with the reported selectivity of MKP5 for p38α MAPK and JNK in addition to the recapitulation of the activities of these MAPKs in MKP5-deficient mice and cells (18, 30). Further evidence that Compound 1 was likely exerting MKP5-selective inhibition was supported by the observation that it enhanced C2C12 myoblast differentiation similar to that seen in MKP5-deficient myoblasts initiated to differentiate. Collectively, these results support the interpretation that Compound 1 acts through MKP5 rather than pervasively inhibiting other MKPs and PTPs.

Our work identifies an allosteric inhibitor of MKP5 and assign it as such through the determination of its co-crystal structure. BCI is proposed to act through an allosteric mechanism to inhibit MKP3 but the assignment of where it binds on MKP3 has been obtained through *in silico* modeling rather than co-crystallographic determination (45). Furthermore, unlike Compound 1 which exhibits a 16-fold reduced potency to MKP1, BCI inhibits MKP3 and MKP1 with relative equipotency. Thus, Compound 1 represents a well-validated starting-point for the development of selective allosteric MKP inhibitors.

Genetic deletion of MKP5 in a mouse model of Duchenne muscular dystrophy rescues the disease, in part by preventing the development of fibrosis, suggesting that MKP5 is a potential therapeutic target for this disease. Here, we uncovered a link between MKP5 and the TGF-β1 pathway, which plays a role in the progression of fibrosis in dystrophic muscle disease (20–22). The evidence that MKP5 is required for TGF-β1 signaling were supported genetically in MKP5-deficient mice and fibroblasts where we showed that MKP5 was required for TGF-β1-induced Smad2 phosphorylation. These data are further substantiated by findings that indicate that MKP5 is required for the actions of TGF-β1 signaling in the lung-derived fibroblasts (46). These data suggest that a MKP5-regulated MAPK-dependent pathway plays a critical role in the activation of Smad2. Similarly, Compound 1 inhibited Smad2 phosphorylation in fibroblasts. The specificity of Compound 1 to act through MKP5 rather than through other MKPs and/or other targets was supported by the lack of observable enhancement in the inhibition of Smad2 phosphorylation or increased MAPK activities in MKP5-deficient cells treated with TGF-β1. We noted that Compound 1 was more effective at enhancing and inhibiting MAPK and Smad2 phosphorylation, respectively in cells as compared with its in vitro inhibitory potency against MKP5. As discussed, the three-pronged inhibitory mechanism for Compound 1 is likely to be engaged in a more unifying context with full-length MAPKs and MKP5 in cells as compared to its in vitro effectiveness. The actions of Compound 1 on MKP5 also results in p38α MAPK activation at concentrations that inhibit Smad2 without affecting either JNK or ERK1/2. These results suggest a MKP5/

p38α MAPK-dependent pathway in the regulation of TGF-β1-induced Smad2 phosphorylation might predominate. More potent MKP5 inhibitors which can be used as tools to further elucidate how interference of this allosteric site disrupts both MKP5 catalysis and MAPK binding will be required to fully understand the mechanistic basis for these effects. In addition, further work will be required to uncover the precise mechanism of how MKP5, and potentially other downstream targets of MKP action, regulate TGF-β1 signaling. Collectively, these findings support the interpretation of a critical role for MKP5 in the TGF-β1 pathway which is a validated target for anti-fibrotic therapy (23, 24, 28). Because fibrosis is the end-stage sequelae in dystrophic muscle disease that results in the loss of muscle function, our data provide insight in to how MKP5 antagonism could offer therapeutic relief to this disease.

In summary, this work has uncovered an allosteric site in MKP5, which represents a new mechanism that may be exploited to specifically inhibit this enzyme and possibly other MKPs. By targeting the MKP5 allosteric site, it is now possible to circumvent the issues that have plagued the development of MKP inhibitors, paving the way for the development of a drug for the treatment of DMD and potentially other fibrotic diseases, such as pulmonary fibrosis, in which MKP5 has been implicated in playing a role (46). Future work will take advantage of the unique chemical scaffold of Compound 1 for functionalization and structure-based optimization focusing on potency and pharmacokinetic parameters. We propose that allosteric modulation of the MKPs is now feasible and will facilitate targeting these enzymes against a variety of human diseases.

MATERIALS AND METHODS

Protein Expression and Purification

The catalytic domain of human MKP5 (MKP5-CD, residues 320-467) and full-length MKP5 (residues 1-482) were inserted into a pET-28a vector for expression. Mutant constructs were generated according to the QuikChange II (Agilent) site directed mutagenesis protocol (primer sequences listed in table S6). Constructs were transformed into BL21 gold (DE3) cells and grown in LB containing 50 μg/mL kanamycin to an OD of 0.8. Protein expression was induced with 1 mM IPTG, and cells were harvested after overnight incubation at 16°C.

Cell pellets were resuspended in lysis buffer containing 20 mM Tris (pH 7.4), 200 mM NaCl, 10% glycerol, 5 mM imidazole, 2 mM β-mercaptoethanol, DNase1, and a complete EDTA-free protease inhibitor. Cells were lysed with a cell disruptor and cellular debris were pelleted by centrifugation. The supernatant was loaded by gravity flow onto a TALON resin column equilibrated in 20 mM Tris (pH 7.4), 200 mM NaCl, 10% glycerol, 5 mM imidazole, 2 mM β-mercaptoethanol and protein was eluted with the addition of 200 mM imidazole. MKP5-CD containing fractions were exchanged into thrombin cleavage buffer (50 mM Tris pH 8.4, 150 mM NaCl, 2.5 mM $CaCl_2$). The N-terminal His-tag was removed by overnight incubation with thrombin at 4°C. After cleavage, the protein was reapplied to a TALON resin column and collected in the flow-through. The protein was concentrated to 12 mg/mL, exchanged into storage buffer (20 mM Tris (pH 7.4), 150 mM NaCl, 5% glycerol, 5 mM dithiothreitol) flash frozen, and stored at −80°C. MKP7-CD (residues 156-301) and MKP3-CD (residues 205-352) were expressed and purified by the same method.

Full-length p38α MAPK was expressed and purified as previously described (47) with the following modifications. Full-length p38α and constitutively-active MKK6 were inserted into a pETDuet-1 vector for expression. Constructs were transformed into BL21 (DE3) cells and grown in Dynamite Broth containing 100 μg/mL ampicillin to an OD of 6.0 (48). Expression of protein was induced with 0.2 mM IPTG and cells were harvested after overnight incubation at 22°C. Cell pellets were resuspended in lysis buffer containing 50 mM Tris (pH 8), 300 mM NaCl, 1 mM NaF, 0.1 mM $NaVO_4$, and a complete EDTA-free protease inhibitor. Cells were lysed by cell disruption and cellular debris were pelleted by centrifugation. Supernatant was loaded onto a 5 mL HiTrap TALON Crude and eluted with a gradient of 0-500 mM imidazole in 20 mM Tris pH 7.4, 200 mM NaCl, and 10% glycerol. Fractions containing p38α were concentrated and further purified by using a Superdex 75 10/300 GL (GE) gel filtration column equilibrated with p38α storage buffer (20 mM Tris pH 7.5, 100 mM NaCl, 2 mM DTT, 20% glycerol). Fractions containing p38α were concentrated to 1.8 mM, flash frozen, and stored at −80°C until use. MKP1-CD (residues 172-314) was expressed and purified by ARVYS Proteins (Trumbull, CT).

High-Throughput MKP5 Inhibitor Screen

The Yale Center for Molecular Discovery small molecule collection was screened for activity against MKP5-CD using a malachite green assay in 384-well format. MKP5-CD and p38α MAPK phosphopeptide (DDE(Nle)(pT)G(pY)VATR) substrate were diluted into PTP buffer (50 mM Tris pH 7.2, 1 mM EDTA, 0.1% β-mercaptoethanol, 0.01% Triton X-100). The screen was performed in two distinct phases. An initial screen against a subset of the compound library was carried out in the following conditions: 1.5 μM MKP5-CD, 25 μM phosphopeptide, 30 min at 37°C. A second follow-up screen was performed with the following modifications: 0.5 μM MKP5-CD, 50 μM phosphopeptide, 15 min at 30°C. Test compounds (20 nL) were dispensed with either an Aquarius (Tecan) pintool system (initial phase) or Echo 550 (Labcyte) acoustic dispenser (follow-up phase). In both phases, the test compound concentration was 20 μM in the 10 μL reaction and the final DMSO was 0.2%. The reaction was stopped by addition of 40 μL 1.6 N HCl containing 0.027% malachite green and 1.68% ammonium molybdate. The plate was incubated for 10-15 min at room temperature to allow color development and absorbance at 620 nm measured. The signal-to-background ratio was calculated from the mean absorbance of vehicle-treated wells with and without enzyme (negative and positive controls; n=32 per condition). Percent inhibition of test wells was calculated from the mean positive and negative controls on each plate. The average S/B and Z' across 449 plates were 4.1 and 0.81, respectively. Plates with Z' less than 0.5 were excluded from further analysis. Wells with percent inhibition ≥ 30% were considered active. Based on this cutoff, the overall hit rate for the screen was 0.2%.

Biophysical Techniques

Binding interactions between MKP5-CD and Compound 1 were carried out using microscale thermophoresis (MST). MST was performed with a Monolith NT.115Pico (NanoTemper) instrument (49). MKP5-CD was labeled for MST using NanoTemper Monolith NT™ Protein Labeling Kit RED-NHS 2nd Generation (#MO-L011). Briefly, MKP5-CD was transferred into the provided labeling buffer and diluted to 20 μM. Dye was added in a 2-fold molar excess and allowed to incubate 30 minutes at room temperature.

Excess dye was removed using the provided column equilibrated in 50 mM Tris pH 8.0, 150 mM NaCl, 0.05% Tween-20. A fixed amount of labeled wild-type or mutant MKP5-CD was combined with up to 200 μM Compound 1 and loaded into premium capillaries. MST experiments were carried out at 40% IR power for 20 seconds. Normalized fluorescence (F_{norm}) values at a given time were plotted against inhibitor concentration and the K_d was determined by fitting with a hyperbolic binding curve. Experiments were performed in triplicate and data are presented as means ± SD. Evaluation of proper protein folding was carried out using circular dichroism. MKP5-CD constructs were diluted to a final volume of 400 μL in storage buffer were analyzed for circular dichroism absorption by an Applied Photophysics Chirascan™ Circular Dichroism spectrophotometer Model 215 (AVIV Instruments, Inc.). Curves for each construct were normalized so that the minimum ellipticity is equal.

Phosphatase Activity Assays

The selection of substrate and assay for each experiment was determined by a number of factors, including method of detection, enzyme-substrate affinity (32, 47, 64, 65) and physiological relevance (table S1). The p38α MAPK phosphopeptide was used for the evaluation of inhibitor potency against wild-type MKP5-CD, mutant MKP5-CD variants, MKP1-CD, and MKP7-CD. As MKP3-CD has very little activity against p38α, it and MKP5-CD were assayed with 6,8-difluoro-4-methylumbelliferyl phosphate (DiFMUP) to allow direct comparison of inhibition(50). Our assays of baseline phosphatase activity of wild-type and mutant MKP5 employed *para*-nitrophenyl phosphate (*p*NPP). Full-length p38α MAPK was used for our steady-state kinetic assays to more completely capture the interactions between Compound 1, MKP5-CD, and its substrate. Finally, in order to execute a stopped-flow fluorescence method to interrogate the transient kinetics of MKP5-CD activity, the fluorescence of the dephosphorylated DiFMUP product (4,6-difluoro-8-methylumbelliferone) was monitored. Compound 1 selected from the screen was tested for activity against MKP1 and MKP5 using the malachite green assay. For wild-type and mutant MKP5-CD, the same conditions for the screening assay were used. For MKP1-CD, the following conditions were used: 1 μM MKP1-CD, 50 μM pTpY, 120 min at 30°C.

For *p*NPP activity assays against MKP5-CD and the MKP5-CD mutants, proteins were diluted to a working concentration and reactions were initiated with 40 μl *p*NPP in reaction buffer to a final concentration of 10 mM *p*NPP, 24 mM HEPES (pH 7.4), 120 mM NaCl, and 5 mM DTT. Reactions were incubated at 37°C for 10 minutes, followed by quench with 1.450 ml of 200 mM NaOH. Reaction progress was assessed by measuring absorbance at 405 nm using a Beckman DU 530 UV/Vis Spectrophotometer and converted to turnover using an extinction coefficient of 17,800 M^{-1} cm^{-1}.

For DiFMUP activity assays, DiFMUP was purchased from ThermoFisher (Lot# 2016387). To determine the kinetics of MKP5 inhibition, 100 nM MKP5-CD and 0-100 μM Compound 1 were combined in DiFMUP reaction buffer (Tris pH 8, 5 mM DTT, 0.05% Tween-20). Reactions were initiated by the addition of DiFMUP to finals concentration of 16, 40, 100, and 250 μm and allowed to proceed at ambient temperature for 30 minutes. Reaction progress was monitored by fluorescence using a Molecular Devices SpectraMax M5 plate

reader with excitation at 358 nm and emission at 450 nm. Initial velocity was determined by fitting to a one-phase exponential reaction progress curve. These velocities were then plotted against DiFMUP concentration and fit to a mixed-mechanism inhibition curve.

Transient Stopped-Flow Kinetic Assay

Stopped-flow experiments were conducted with a KinTek SF-2001 apparatus. To determine the rate of the dephosphorylation reaction, fluorescence was monitored with 358 nm excitation and an output filter at 450 nm. MKP5-CD (in and out of the presence of inhibitor) and DiFMUP were diluted in the aforementioned DiFMUP reaction buffer plus 5% DMSO. The enzyme and substrate solutions were mixed to final concentrations of 10 μM MKP5-CD, 250-1000 μM DiFMUP, and 0-40 μM inhibitor. Data were then fit to a single exponential burst kinetics curve.

Phosphate Sensor Steady State Kinetic Assay

The phosphate sensor (PS) protein was purchased from Life Technologies (Lot # 1962036B). To characterize the activity of MKP5-CD against full length p38α MAPK, 5 nM MKP5-CD and 0.5 μM PS were combined in 50 mM Tris (pH 7.6), 25 mM NaCl, 0.01% Triton X-100, and 0.5 mM DTT and added to a Corning #4511 384-well plate. Using an Echo 550 liquid handler (LabCyte Inc.), either 25 μM Compound 1 or neat DMSO were added to a final DMSO concentration of 0.2%. Reactions were initiated with up to 150 μM p38α MAPK and allowed to proceed at ambient temperature for 20 minutes. Fluorescence was continuously monitored by Tecan Infinite M1000 with excitation at 425 ± 5 nm and emission at 454 ± 5 nm. Raw fluorescence was converted to phosphate release using a standard curve generated the same day as kinetic experiments. The initial velocity was determined for each well based on reaction progress in the first 120 seconds. These velocities were then plotted against substrate concentration and fit to a mixed-mechanism inhibition curve (31).

Crystallization and Structure Determination

In order to co-crystallize wild-type MKP5-CD with Compound 1, the compound was added to a concentration of 5 mM and allowed to bind overnight at 4°C with shaking. Initial screening was carried out with Hampton Research Crystal Screen 1, Crystal Screen 2, and Index Screen. Subsequent rounds of optimization yielded the following crystallization conditions. Hanging drop vapor diffusion was used with the well solution 100 mM HEPES pH 7.5, 200 mM ammonium acetate, 25% (w/v) PEG 3350 and a drop with a 4:1 volume of MKP5-CD:**1** and well solution. Crystallization experiments were dispensed using a Mosquito (TTP Labtech) liquid handler and crystal growth was monitored using the RockImager R-1000 (Formulatrix). Thin plates formed within two days, were transferred to cryoprotectant of well solution plus 3% PEG 3350, and flash frozen in liquid nitrogen. Diffraction data were collected on the ADSC Q315r CCD detector at the NE-CAT 24-ID-E beamline at the Advanced Photon Source at Argonne National Laboratories. The data were collected to a resolution of 2.7 Å from a single crystal at a wavelength of 0.97918 Å. The data were indexed, integrated, and scaled using XDS (51). The data was phased by molecular replacement with chain A of the MKP5-CD apo structure (32) (PDB accession

1ZZW) with all waters and heteroatoms removed using Phaser (52). The structure was improved through rounds of refinement and model building using Phenix.Refine (53) and Coot (54), respectively. Finally, the structure was validated with MolProbity (55). 99.9% of phi and psi angles are found in the favored or allowed regions of the Ramachandran plot. Contacts between Compound **1** and MKP5-CD were identified with LigPlot+ (56). Crystallographic data and refinement statistics are shown in Supplemental table 1.

The volume of the active site of MKP5 (namely, the pocket containing Cys^{408}) was determined using CAVER Analyst (57) Cavity Computation tool. Cavities were defined by an inner probe of 1.05 Å, an outer probe of 5 Å and clipped by the sphere of radius 5 Å centered on the sulfur atom of Cys^{408}. Active site volumes for wild-type MKP5-CD:Compound 1 and the apo structure of MKP5 (32) were compared by two-tailed one-sample *t*-test.

Multiple Sequence Alignment and Structural Modeling

The primary sequences of twelve human DUSP PTP domains were obtained from Uniprot (58) and aligned with Geneious (v10.2.2) (59). Similarity to MKP5 was determined by BLOSUM62 score. The structures of p38α MAPK (42) (PDB accession 1R39) and MKP5-CD:Compound 1 were superposed on the structure of the complex of JNK1 and MKP7-CD (41) (PDB accession 4YR8) or VHR (43) (PDB accession 1J4X) using PyMOL (60). The root-mean-square deviations for these alignments were 1.903, 0.921, and 1.033 Å, respectively.

Cell culture

C2C12 myoblasts were obtained from ATCC and cultured as described previously (18). Wild type (*Mkp5*$^{+/+}$) and MKP5-deficient (*Mkp5*$^{-/-}$) mouse embryo fibroblasts (MEFs) were generated from female mice at days 13-14 of pregnancy and established by spontaneous immortalization. C2C12 myoblasts and MEFs were treated with Compound 1 overnight followed by 4 h serum starvation and either harvested or stimulated with TGF-β1. For cell proliferation assays, C2C2 myoblasts were plated in growth medium (10%FBS, 1% Pen/strep, 1% Sodium pyruvate) and the next day treated with either DMSO as vehicle or Compound 1 at the indicated concentrations. Cells were incubated for 72 hr and in the last 1 hr of incubation cells were treated with 10 μM of 5-Bromo-2'- dexoyuridine (Sigma-Aldrich #B9285). Cells were fixed, stained with anti-BrdU antibodies (1:50 in 5% goat serum) to detect for the incorporation of BrdU and counter-stained with DAPI for the detection of nuclei. The rate of proliferation was determined by counting the percentage of BrdU-positive cells per total number of DAPI-positive cells per field from at least 10 separate fields. For myoblast differentiation assays, C2C12 myoblasts were plated in growth medium, prior to the initiation of differentiation by culturing cells in DMEM containing 0.1% FBS, 5 μg/mL insulin and 5 μg/mL selenium. Cells were treated either with DMSO as vehicle or Compound 1 at the indicated concentration. Cells were differentiated for 72 hr after which cells were stained with anti-MF20 antibodies (1:50 in 5% goat serum) for the expression of myosin heavy chain and DAPI for nuclei. The number of nuclei per myotube was determined from at least 10 fields to calculate the fusion index. Fusion index is calculated as

a percentage of nuclei within myotubes containing at least 2 nuclei as a ratio of total nuclei in the field. Significance was established by two-tailed *t*-test.

Immunoblotting

For immunoblotting, C2C12 myoblasts or *Mkp5*$^{+/+}$ and *Mkp5*$^{-/-}$ fibroblasts were lysed on ice in lysis buffer containing 150 mM NaCl, 50 mM Tris-HCl (pH 7.8), 1 mM EDTA, 1% Nonidet P-40, 1 mM Na_3VO_4, 10 mM NaF, 1 mM DTT, 1 mM benzamidine, 1 mM PMSF, 1 μg/ml pepstatin A, 5 μg/ml aprotinin, and 5 μg/ml leupeptin for 30 min and clarified by centrifugation at 20,800 x *g* at 4 °C for 20 min. Protein concentration was determined using BCA reagent according to the manufacturer's instructions (Pierce). Recombinant human TGF-β1 (240-B-002) was purchased from R&D Systems. For phospho-MAPK and MAPK immunoblotting, lysates were resolved by SDS-PAGE and transferred onto nitrocellulose membranes (Bio-Rad). Membranes were blocked with 5% nonfat dry milk or 5% BSA in Tris-buffered saline/Tween 20 (TBS-T) for 1 h at room temperature or overnight at 4 °C. Primary antibodies were diluted in 5% BSA or 5% nonfat dry milk in TBS-T. The following primary antibodies were used: phospho-p38α MAPK (Thr^{180}/Tyr^{182}) (9125), phospho-JNK1/2 (Thr^{183}/Tyr^{185}) (4668), and phospho-ERK1/2 (Thr^{202}/Tyr^{204}) (9101), Smad2 (3103) or phospho-Smad2 (Ser$^{465/467}$) (3108) were obtained from Cell Signaling Technologies. ERK1/2 (9107), and JNK (3708) were purchased from Cell Signaling Technologies and p38α MAPK (81621) was obtained from Santa Cruz Biotechnology. MAPK and Smad2 activation were calculated as the ratio of the indicated phosphorylated MAPK or phosphorylated Smad2 to total MAPK or Smad2, respectively by direct fluorescence quantitation using the Odyssey CLx Imaging System. Images were processed with the LI-COR Image Studio Software.

Animal Studies

MKP5-deficient mice were provided by Dr. Flavell (Yale University School of Medicine) (11) and were maintained as previously described (18). Yale University Institutional Animal Care and Use Committee approved all procedures. Skeletal muscle injury was induced by intramuscular injection of 300 μl cardiotoxin (Sigma-Aldrich, 0.1 mg/ml in PBS) into the gastrocnemius/soleus muscles, after anesthesia by administration of 10 mg/kg ketamine and 1 mg/kg xylazine. Soleus muscle from uninjured and at 4 and 10 days after injury was removed and rapidly frozen in liquid nitrogen and stored at −80°C for subsequent biochemical analyses. For immunoblotting, soleus muscles were homogenized and lysed on ice in lysis buffer containing 100 mM Tris HCl (pH 7.4) and 25 mM EDTA. C2C12 myoblasts were lysed on ice in lysis buffer containing 50 mM Tris-HCl (pH 7.8), 150 mM NaCl, 1 mM EDTA, 1% Triton X-100, 0.5% sodium deoxycholate, 0.1% SDS. Lysis buffers were supplemented with protease and phosphatase inhibitors (1 mM Na_3VO_4, 10 mM NaF, 1 mM benzamidine, 1 mM phenylmethylsulfonyl fluoride, 1 μg/ml pepstatin A, 5 μg/ml aprotinin, 5 μg/ml leupeptin). Tissue or cell lysates were incubated at 4°C for 30 min and clarified by centrifugation at 14,000 rpm at 4°C for 10 min. Lysates were resolved by SDS-PAGE, transferred to nitrocellulose membranes and immunoblotted with either antibodies to either Smad2 or phospho-Smad2. Differences between genotypes were assessed by a Student's *t* test or analysis of variance (ANOVA) with Tukey's multiple comparisons test using Prism software (GraphPad Software).

Quantification and statistical analysis

All reported p values are from two-tailed Student's t test unless otherwise indicated in the relevant figure legend. Statistics including t, degrees of freedom and other parameters may be found in the figure legends. Significance was defined as a p value less than 0.05.

Supplementary Material

Refer to Web version on PubMed Central for supplementary material.

Acknowledgments:

We thank Dr. Schlessinger for providing access to the NanoTemper Monolith NT.115 Microscale Thermophoresis. Resources of the CCMI Macromolecular X-ray Crystallography Facility were used for crystallographic experiments.

Funding: This work is based upon research conducted at the Northeastern Collaborative Access Team beamlines, which are funded by the National Institute of General Medical Sciences from the National Institutes of Health (P30 GM124165). This research used resources of the Advanced Photon Source, a U.S. Department of Energy (DOE) Office of Science User Facility operated for the DOE Office of Science by Argonne National Laboratory under Contract No. DE-AC02-06CH11357. This research used resources of the National Synchrotron Light Source, a U.S. Department of Energy (DOE) Office of Science User Facility operated for the DOE Office of Science by Brookhaven National Laboratory under Contract No. DE-AC02-98CH10886. A.M.B. was supported by NIH grant R01AR66003, Blavatnik Innovations Award and the Program in Innovative Therapeutics for Connecticut's Health. Z.T.K.G. was supported by NIH grant T32 AI055403. S.S. was supported by NIG grant T32 GM06754. J.A.E. was supported by NIH grant R35 GM122473.

REFERENCES AND NOTES

1. Cargnello M, Roux PP, Activation and function of the MAPKs and their substrates, the MAPK-activated protein kinases. Microbiol Mol Biol Rev 75, 50–83 (2011); published online EpubMar (10.1128/mmbr.00031-10). [PubMed: 21372320]
2. Hotamisligil GS, Davis RJ, Cell Signaling and Stress Responses. Cold Spring Harbor perspectives in biology 8, (2016); published online EpubOct 03 (10.1101/cshperspect.a006072).
3. Wang Y, Mitogen-activated protein kinases in heart development and diseases. Circulation 116, 1413–1423 (2007); published online EpubSep 18 (10.1161/CIRCULATIONAHA.106.679589). [PubMed: 17875982]
4. Lawan A, Bennett AM, Mitogen-Activated Protein Kinase Regulation in Hepatic Metabolism. Trends in endocrinology and metabolism: TEM 28, 868–878 (2017); published online EpubDec (10.1016/j.tem.2017.10.007). [PubMed: 29128158]
5. Shi H, Bennett AM, in Muscular Dystrophy, Hedge M, Ankala A, Eds. (InTech, 2012), chap. 8, pp. 159–172.
6. Wagner EF, Nebreda AR, Signal integration by JNK and p38 MAPK pathways in cancer development. Nat Rev Cancer 9, 537–549 (2009); published online EpubAug (10.1038/nrc2694). [PubMed: 19629069]
7. Caunt CJ, Keyse SM, Dual-specificity MAP kinase phosphatases (MKPs): shaping the outcome of MAP kinase signalling. The FEBS journal 280, 489–504 (2013); published online EpubJan (10.1111/j.1742-4658.2012.08716.x). [PubMed: 22812510]
8. Farooq A, Zhou MM, Structure and regulation of MAPK phosphatases. Cellular signalling 16, 769–779 (2004); published online EpubJul (10.1016/j.cellsig.2003.12.008). [PubMed: 15115656]
9. Zhang YY, Wu JW, Wang ZX, A distinct interaction mode revealed by the crystal structure of the kinase p38alpha with the MAPK binding domain of the phosphatase MKP5. Science signaling 4, ra88 (2011); published online EpubDec 20 (10.1126/scisignal.2002241). [PubMed: 22375048]
10. Camps M, Nichols A, Gillieron C, Antonsson B, Muda M, Chabert C, Boschert U, Arkinstall S, Catalytic Activation of the Phosphatase MKP-3 by ERK2 Mitogen-Activated Protein Kinase. Science 280, 1262–1264 (1998). [PubMed: 9596579]

11. Zhang Y, Blattman JN, Kennedy NJ, Duong J, Nguyen T, Wang Y, Davis RJ, Greenberg PD, Flavell RA, Dong C, Regulation of innate and adaptive immune responses by MAP kinase phosphatase 5. Nature 430, 793–797 (2004); published online EpubAug 12 (10.1038/nature02764). [PubMed: 15306813]
12. Qian F, Deng J, Cheng N, Welch EJ, Zhang Y, Malik AB, Flavell RA, Dong C, Ye RD, A non-redundant role for MKP5 in limiting ROS production and preventing LPS-induced vascular injury. The EMBO journal 28, 2896–2907 (2009); published online EpubOct 7 (10.1038/emboj.2009.234). [PubMed: 19696743]
13. Png CW, Weerasooriya M, Guo J, James SJ, Poh HM, Osato M, Flavell RA, Dong C, Yang H, Zhang Y, DUSP10 regulates intestinal epithelial cell growth and colorectal tumorigenesis. Oncogene 35, 206–217 (2016); published online EpubJan 14 (10.1038/onc.2015.74). [PubMed: 25772234]
14. Cheng Q, Zhang Q, Xu X, Yin L, Sun L, Lin X, Dong C, Pan W, MAPK phosphotase 5 deficiency contributes to protection against blood-stage Plasmodium yoelii 17XL infection in mice. Journal of immunology (Baltimore, Md. : 1950) 192, 3686–3696 (2014); published online EpubApr 15 (10.4049/jimmunol.1301863).
15. Lawan A, Min K, Zhang L, Canfran-Duque A, Jurczak MJ, Camporez JPG, Nie Y, Gavin TP, Shulman GI, Hernandez-Fernando C, Bennett AM, Skeletal Muscle-Specific Deletion of MKP-1 Reveals a p38 MAPK/JNK/Akt Signaling Node that Regulates Obesity-Induced Insulin Resistance. Diabetes, (2018); published online EpubJan 9 (10.2337/db17-0826).
16. Choi HR, Kim WK, Kim EY, Han BS, Min JK, Chi SW, Park SG, Bae KH, Lee SC, Dual-specificity phosphatase 10 controls brown adipocyte differentiation by modulating the phosphorylation of p38 mitogen-activated protein kinase. PloS one 8, e72340 (2013) 10.1371/journal.pone.0072340). [PubMed: 23977283]
17. Shi H, Boadu E, Mercan F, Le AM, Flach RJ, Zhang L, Tyner KJ, Olwin BB, Bennett AM, MAP kinase phosphatase-1 deficiency impairs skeletal muscle regeneration and exacerbates muscular dystrophy. FASEB journal : official publication of the Federation of American Societies for Experimental Biology 24, 2985–2997 (2010); published online EpubAug (10.1096/fj.09-150045). [PubMed: 20371627]
18. Shi H, Verma M, Zhang L, Dong C, Flavell RA, Bennett AM, Improved regenerative myogenesis and muscular dystrophy in mice lacking Mkp5. The Journal of clinical investigation 123, 2064–2077 (2013); published online EpubMay (10.1172/JCI64375). [PubMed: 23543058]
19. Hoffman EP, Brown RH Jr., Kunkel LM, Dystrophin: the protein product of the Duchenne muscular dystrophy locus. Cell 51, 919–928 (1987); published online EpubDec 24 ([PubMed: 3319190]
20. Serrano AL, Munoz-Canoves P, Regulation and dysregulation of fibrosis in skeletal muscle. Exp Cell Res 316, 3050–3058 (2010); published online EpubNov 1 (10.1016/j.yexcr.2010.05.035). [PubMed: 20570674]
21. Lieber RL, Ward SR, Cellular mechanisms of tissue fibrosis. 4. Structural and functional consequences of skeletal muscle fibrosis. Am J Physiol Cell Physiol 305, C241–252 (2013); published online EpubAug 1 (10.1152/ajpcell.00173.2013). [PubMed: 23761627]
22. Li Y, Foster W, Deasy BM, Chan Y, Prisk V, Tang Y, Cummins J, Huard J, Transforming growth factor-beta1 induces the differentiation of myogenic cells into fibrotic cells in injured skeletal muscle: a key event in muscle fibrogenesis. Am J Pathol 164, 1007–1019 (2004); published online EpubMar ([PubMed: 14982854]
23. Spinazzola JM, Kunkel LM, Pharmacological therapeutics targeting the secondary defects and downstream pathology of Duchenne muscular dystrophy. Expert Opin Orphan Drugs 4, 1179–1194 (2016) 10.1080/21678707.2016.1240613). [PubMed: 28670506]
24. Zhou L, Lu H, Targeting fibrosis in Duchenne muscular dystrophy. J Neuropathol Exp Neurol 69, 771–776 (2010); published online EpubAug (10.1097/NEN.0b013e3181e9a34b). [PubMed: 20613637]
25. Zhang ZY, Drugging the Undruggable: Therapeutic Potential of Targeting Protein Tyrosine Phosphatases. Acc Chem Res 50, 122–129 (2017); published online EpubJan 17 (10.1021/acs.accounts.6b00537). [PubMed: 27977138]

26. Chen YP, LaMarche MJ, Chan HM, Fekkes P, Garcia-Fortanet J, Acker MG, Antonakos B, Chen CH, Chen Z, Cooke VG, Dobson JR, Deng Z, Fei F, Firestone B, Fodor M, Fridrich C, Gao H, Grunenfelder D, Hao HX, Jacob J, Ho S, Hsiao K, Kang ZB, Karki R, Kato M, Larrow J, La Bonte LR, Lenoir F, Liu G, Liu S, Majumdar D, Meyer MJ, Palermo M, Perez L, Pu M, Price E, Quinn C, Shakya S, Shultz MD, Slisz J, Venkatesan K, Wang P, Warmuth M, Williams S, Yang G, Yuan J, Zhang JH, Zhu P, Ramsey T, Keen NJ, Sellers WR, Stams T, Fortin PD, Allosteric inhibition of SHP2 phosphatase inhibits cancers driven by receptor tyrosine kinases. Nature 535, 148–152 (2016); published online EpubJun 29 (10.1038/nature18621). [PubMed: 27362227]
27. Krishnan N, Koveal D, Miller DH, Xue B, Akshinthala SD, Kragelj J, Jensen MR, Gauss C-M, Page R, Blackledge M, Muthuswamy SK, Peti W, Tonks NK, Targeting the disordered C terminus of PTP1B with an allosteric inhibitor. Nature chemical biology 10, 558 (2014); published online Epub05/20/online (10.1038/nchembio.152810.1038/nchembio.1528https://www.nature.com/articles/nchembio.1528#supplementary-informationhttps://www.nature.com/articles/nchembio.1528#supplementary-information). [PubMed: 24845231]
28. Mah JK, Current and emerging treatment strategies for Duchenne muscular dystrophy. Neuropsychiatr Dis Treat 12, 1795–1807 (2016)10.2147/NDT.S93873). [PubMed: 27524897]
29. Tautz L, Sergienko EA, High-throughput screening for protein tyrosine phosphatase activity modulators. Methods Mol Biol 1053, 223–240 (2013)10.1007/978-1-62703-562-0_14). [PubMed: 23860657]
30. Tanoue T, Moriguchi T, Nishida E, Molecular cloning and characterization of a novel dual specificity phosphatase, MKP-5. The Journal of biological chemistry 274, 19949–19956 (1999); published online EpubJul 9 ([PubMed: 10391943]
31. Copeland RA, in Evaluation of Enzyme Inhibitors in Drug Discovery. (A John Wiley & Sons, Inc., 2013), chap. 3, pp. 57–121.
32. Jeong DG, Yoon T-S, Kim JH, Shim MY, Jung S-K, Son JH, Ryu SE, Kim SJ, Crystal Structure of the Catalytic Domain of Human MAP Kinase Phosphatase 5: Structural Insight into Constitutively Active Phosphatase. Journal of Molecular Biology 360, 946–955 (2006). [PubMed: 16806267]
33. Tao X, Tong L, Crystal structure of the MAP kinase binding domain and the catalytic domain of human MKP5. Protein Sci 16, 880–886 (2007); published online EpubMay 1, 2007 (10.1110/ps.062712807). [PubMed: 17400920]
34. Jia Z, Barford D, Flint A, Tonks N, Structural basis for phosphotyrosine peptide recognition by protein tyrosine phosphatase 1B. Science 268, 1754–1758 (1995)10.1126/science.7540771). [PubMed: 7540771]
35. Lu C, Liu X, Zhang CS, Gong H, Wu JW, Wang ZX, Structural and Dynamic Insights into the Mechanism of Allosteric Signal Transmission in ERK2-Mediated MKP3 Activation. Biochemistry 56, 6165–6175 (2017); published online EpubNov 21 (10.1021/acs.biochem.7b00827). [PubMed: 29077400]
36. Cohn RD, van Erp C, Habashi JP, Soleimani AA, Klein EC, Lisi MT, Gamradt M, ap Rhys CM, Holm TM, Loeys BL, Ramirez F, Judge DP, Ward CW, Dietz HC, Angiotensin II type 1 receptor blockade attenuates TGF-beta-induced failure of muscle regeneration in multiple myopathic states. Nat Med 13, 204–210 (2007); published online EpubFeb (10.1038/nm1536). [PubMed: 17237794]
37. Shi Y, Massague J, Mechanisms of TGF-beta signaling from cell membrane to the nucleus. Cell 113, 685–700 (2003); published online EpubJun 13 ([PubMed: 12809600]
38. Luo L, Parrish CA, Nevins N, McNulty DE, Chaudhari AM, Carson JD, Sudakin V, Shaw AN, Lehr R, Zhao H, Sweitzer S, Lad L, Wood KW, Sakowicz R, Annan RS, Huang PS, Jackson JR, Dhanak D, Copeland RA, Auger KR, ATP-competitive inhibitors of the mitotic kinesin KSP that function via an allosteric mechanism. Nature chemical biology 3, 722 (2007); published online Epub10/07/online (10.1038/nchembio.2007.3410.1038/nchembio.2007.34https://www.nature.com/articles/nchembio.2007.34#supplementary-informationhttps://www.nature.com/articles/nchembio.2007.34#supplementary-information). [PubMed: 17922005]
39. Alphey MS, Pirrie L, Torrie LS, Boulkeroua WA, Gardiner M, Sarkar A, Maringer M, Oehlmann W, Brenk R, Scherman MS, McNeil M, Rejzek M, Field RA, Singh M, Gray D, Westwood NJ, Naismith JH, Allosteric Competitive Inhibitors of the Glucose-1-phosphate Thymidylyltransferase (RmlA) from Pseudomonas aeruginosa. ACS Chemical Biology 8, 387–396 (2013); published online Epub2013/02/15 (10.1021/cb300426u). [PubMed: 23138692]

40. Wei J, Leit S, Kuai J, Therrien E, Rafi S, Harwood HJ, DeLaBarre B, Tong L, An allosteric mechanism for potent inhibition of human ATP-citrate lyase. Nature 568, 566–570 (2019); published online Epub2019/04/01 (10.1038/s41586-019-1094-6). [PubMed: 30944472]
41. Liu X, Zhang CS, Lu C, Lin SC, Wu JW, Wang ZX, A conserved motif in JNK/p38-specific MAPK phosphatases as a determinant for JNK1 recognition and inactivation. Nat Commun 7, 10879 (2016); published online EpubMar 18 (10.1038/ncomms10879). [PubMed: 26988444]
42. Patel SB, Cameron PM, Frantz-Wattley B, O'Neill E, Becker JW, Scapin G, Lattice stabilization and enhanced diffraction in human p38 alpha crystals by protein engineering. Biochimica et biophysica acta 1696, 67–73 (2004); published online EpubJan 14 ([PubMed: 14726206]
43. Schumacher MA, Todd JL, Rice AE, Tanner KG, Denu JM, Structural basis for the recognition of a bisphosphorylated MAP kinase peptide by human VHR protein Phosphatase. Biochemistry 41, 3009–3017 (2002); published online EpubMar 5 [PubMed: 11863439]
44. Cui DS, Beaumont V, Ginther PS, Lipchock JM, Loria JP, Leveraging Reciprocity to Identify and Characterize Unknown Allosteric Sites in Protein Tyrosine Phosphatases. Journal of Molecular Biology 429, 2360–2372 (2017); published online Epub2017/07/21/ (10.1016/j.jmb.2017.06.009). [PubMed: 28625849]
45. Molina G, Vogt A, Bakan A, Dai W, Queiroz de Oliveira P, Znosko W, Smithgall TE, Bahar I, Lazo JS, Day BW, Tsang M, Zebrafish chemical screening reveals an inhibitor of Dusp6 that expands cardiac cell lineages. Nature chemical biology 5, 680–687 (2009); published online EpubSep (10.1038/nchembio.190). [PubMed: 19578332]
46. Xylourgidis N, Min K, Ahangari F, Yu G, Herazo-Maya JD, Karampitsakos T, Aidinis V, Binzenhofer L, Bouros D, Bennett AM, Kaminski N, Tzouvelekis A, Role of dual-specificity protein phosphatase DUSP10/MKP-5 in pulmonary fibrosis. American journal of physiology. Lung cellular and molecular physiology 317, L678–L689 (2019); published online EpubNov 1 (10.1152/ajplung.00264.2018). [PubMed: 31483681]
47. Zhang YY, Mei ZQ, Wu JW, Wang ZX, Enzymatic activity and substrate specificity of mitogen-activated protein kinase p38alpha in different phosphorylation states. The Journal of biological chemistry 283, 26591–26601 (2008); published online EpubSep 26 (10.1074/jbc.M801703200). [PubMed: 18669639]
48. Taylor T, Denson J-P, Esposito D, in Heterologous Gene Expression in E.coli: Methods and Protocols, Burgess-Brown NA, Ed. (Springer New York, New York, NY, 2017), pp. 65–82.
49. Jerabek-Willemsen M, André T, Wanner R, Roth HM, Duhr S, Baaske P, Breitsprecher D, MicroScale Thermophoresis: Interaction analysis and beyond. J Mol Struct 1077, 101–113 (2014); published online Epub2014/12/05/ (10.1016/j.molstruc.2014.03.009).
50. Muda M, Theodosiou A, Rodrigues N, Boschert U, Camps M, Gillieron C, Davies K, Ashworth A, Arkinstall S, The Dual Specificity Phosphatases M3/6 and MKP-3 Are Highly Selective for Inactivation of Distinct Mitogen-activated Protein Kinases. Journal of Biological Chemistry 271, 27205–27208 (1996); published online EpubNovember 1, 1996 (10.1074/jbc.271.44.27205). [PubMed: 8910287]
51. Kabsch W, Xds. Acta Crystallogr D 66, 125–132 (2010); published online EpubFeb (10.1107/S0907444909047337). [PubMed: 20124692]
52. McCoy AJ, Grosse-Kunstleve RW, Adams PD, Winn MD, Storoni LC, Read RJ, Phaser crystallographic software. J Appl Crystallogr 40, 658–674 (2007); published online EpubAug 1 (10.1107/S0021889807021206). [PubMed: 19461840]
53. Adams PD, Afonine PV, Bunkoczi G, Chen VB, Davis IW, Echols N, Headd JJ, Hung LW, Kapral GJ, Grosse-Kunstleve RW, McCoy AJ, Moriarty NW, Oeffner R, Read RJ, Richardson DC, Richardson JS, Terwilliger TC, Zwart PH, PHENIX: a comprehensive Python-based system for macromolecular structure solution. Acta Crystallogr D 66, 213–221 (2010); published online EpubFeb (10.1107/S0907444909052925). [PubMed: 20124702]
54. Emsley P, Lohkamp B, Scott WG, Cowtan K, Features and development of Coot. Acta Crystallogr D 66, 486–501 (2010); published online EpubApr (10.1107/S0907444910007493). [PubMed: 20383002]
55. Chen VB, Arendall WB 3rd, Headd JJ, Keedy DA, Immormino RM, Kapral GJ, Murray LW, Richardson JS, Richardson DC, MolProbity: all-atom structure validation for macromolecular

crystallography. Acta Crystallogr D 66, 12–21 (2010); published online EpubJan (10.1107/S0907444909042073). [PubMed: 20057044]

56. Laskowski RA, Swindells MB, LigPlot+: multiple ligand-protein interaction diagrams for drug discovery. J Chem Inf Model 51, 2778–2786 (2011); published online EpubOct 24 (10.1021/ci200227u). [PubMed: 21919503]
57. Kozlikova B, Sebestova E, Sustr V, Brezovsky J, Strnad O, Daniel L, Bednar D, Pavelka A, Manak M, Bezdeka M, Benes P, Kotry M, Gora A, Damborsky J, Sochor J, CAVER Analyst 1.0: graphic tool for interactive visualization and analysis of tunnels and channels in protein structures. Bioinformatics 30, 2684–2685 (2014); published online EpubSep 15 (10.1093/bioinformatics/btu364). [PubMed: 24876375]
58. C. The UniProt, UniProt: the universal protein knowledgebase. Nucleic Acids Res 45, D158–D169 (2017); published online EpubJan 4 (10.1093/nar/gkw1099). [PubMed: 27899622]
59. Kearse M, Moir R, Wilson A, Stones-Havas S, Cheung M, Sturrock S, Buxton S, Cooper A, Markowitz S, Duran C, Thierer T, Ashton B, Meintjes P, Drummond A, Geneious Basic: an integrated and extendable desktop software platform for the organization and analysis of sequence data. Bioinformatics 28, 1647–1649 (2012); published online EpubJun 15 (10.1093/bioinformatics/bts199). [PubMed: 22543367]
60. Schrodinger L. (2015). The PyMOL Molecular Graphics System, Version 2.0 Schrödinger, LLC.
61. Copeland RA (2013). Reversible Modes of Inhibitor Interactions with Enzymes In Evaluation of Enzyme Inhibitors in Drug Discovery, Copeland RA, ed. (A John Wiley & Sons, Inc.).
62. Prim D, and Kirsch G (1995). Synthesis of New 3-Methylthio-4, 5, 6, 7-tetrahydro Benzo[c]thiophene-4-ones. Synthetic Communications 25, 2449–2455.
63. Weinstein AB, and Ellman JA (2016). Convergent Synthesis of Diverse Nitrogen Heterocycles via Rh(III)-Catalyzed C–H Conjugate Addition/Cyclization Reactions. Organic Letters 18, 3294–3297. [PubMed: 27337641]
64. Li R, Xie DD, Dong JH, Li H, Li KS, Su J, Chen LZ, Xu YF, Wang HM, Gong Z, Cui GY, Yu X, Wang K, Yao W, Xin T, Li MY, Xiao KH, An XF, Huo Y, Xu ZG, Sun JP, Pang Q, Molecular mechanism of ERK dephosphorylation by striatal-enriched protein tyrosine phosphatase. J Neurochem 128, 315–329 (2014); published online EpubJan (10.1111/jnc.12463). [PubMed: 24117863]
65. PTP1B Assay Kit, #539736 (MilliPore-Sigma).

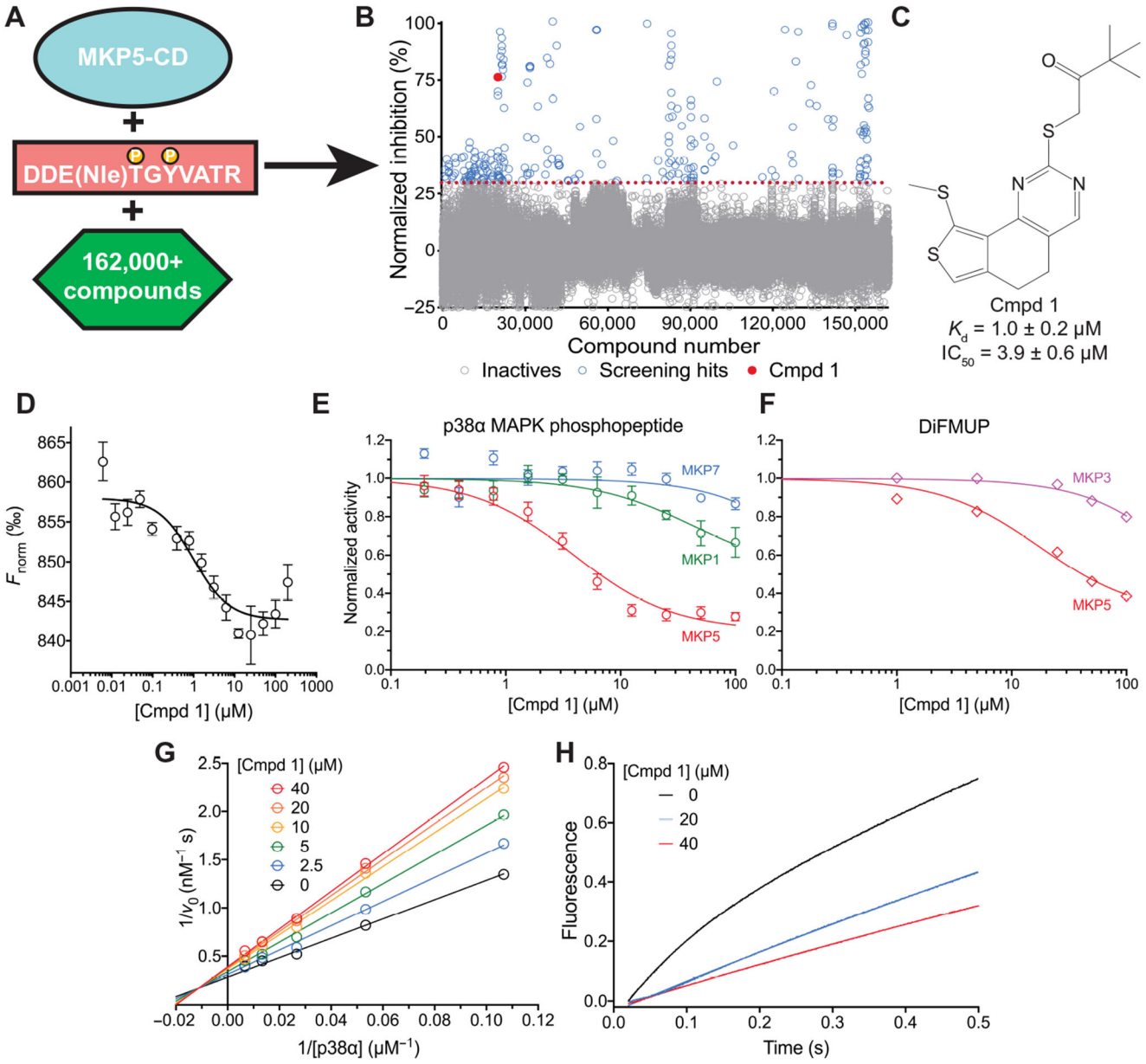

Figure 1. High-throughput screen yields micromolar inhibitor of MKP5.

a, Schematic of high-throughput screen to identify MKP5 inhibitors. A malachite green assay was used to quantify phosphate release from a reaction mixture containing 1 μM of MKP5-CD, 25 μM p38α MAPK phosphopeptide (pTpY), and 20 μM of each compound. **b**, Summary of screen results. Red dotted line represents 30% threshold for hit identification. Red circle indicates compound (Cmpd) 1. **c,** Chemical structure of Cmpd 1 and shown below the calculated K_d and IC_{50} assayed against MKP5-CD. **d,** Microscale thermophoresis assay of MKP5-CD:Cmpd 1 binding. Curve-fit to hyperbolic binding-equation; F_{norm} – Normalized fluorescence. **e-f,** Assays of MKP inhibition. Substrates were selected for optimal MKP activity; MKPs active against p38α MAPK, MKP7 and MKP1, were assayed with the p38α MAPK phosphopeptide, MKP3, which has no phosphatase activity against

p38α MAPK, was assayed against DiFMUP. Data are normalized against DMSO control and fit to hyperbolic inhibition equation. **g,** Lineweaver-Burk plot of phosphate sensor kinetic assay of Cmpd 1 inhibition of full-length p38α MAPK dephosphorylation. Data were fit to straight lines intersecting at a single point. Nonlinear regression of the same data is shown in fig. S6c. **h**, Transient kinetic assay of MKP5-CD activity against DiFMUP in the absence and presence of Cmpd 1. Data are fit to single exponential equation with burst. Data are presented as mean ± SD (**d**-**f**) or mean (**g**-**h**) and are the product of three (**d**-**g**) or 5-6 (**h**) independent experiments.

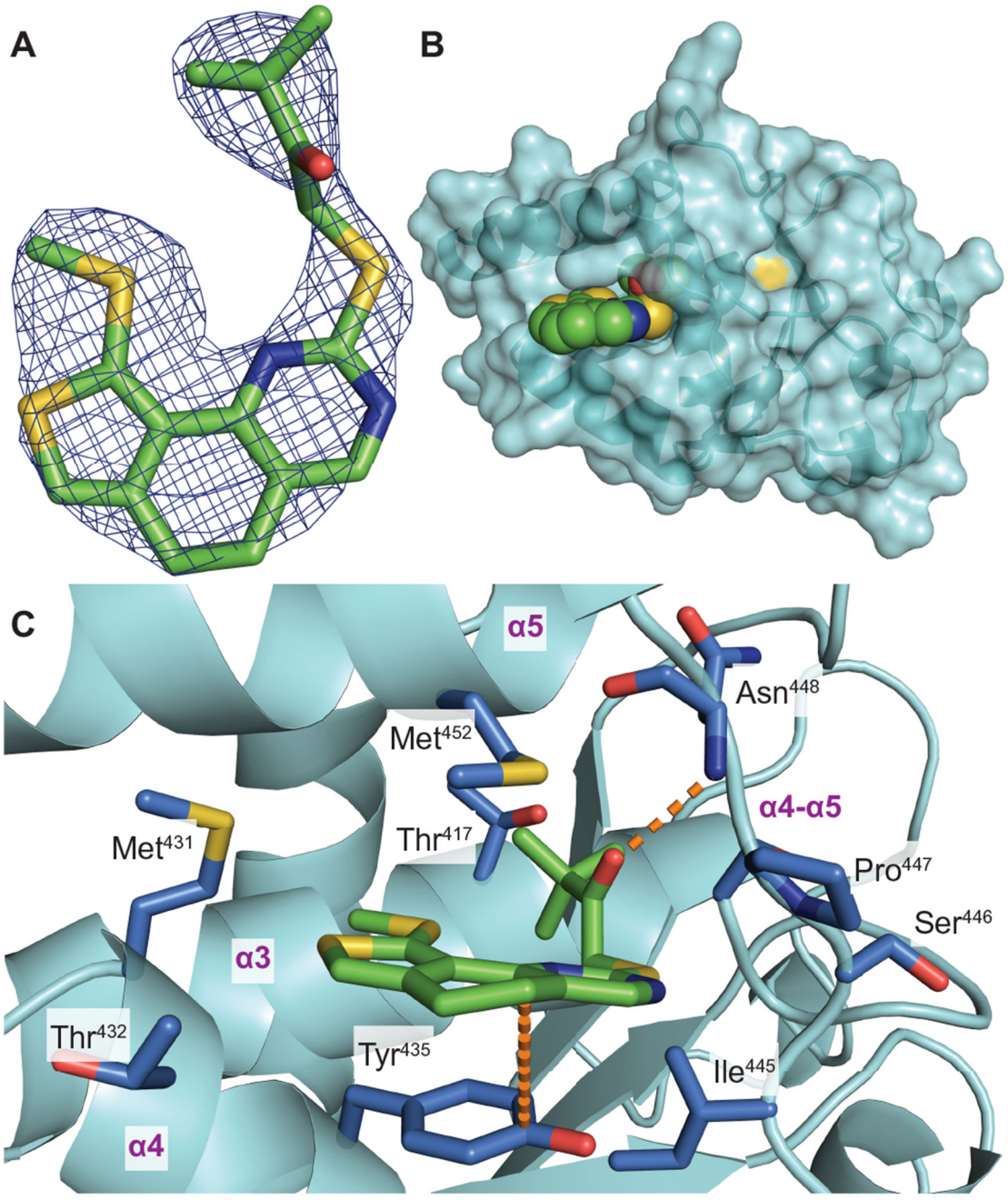

Figure 2. X-ray crystal structure of MKP5-CD in complex with Compound 1.

a, $2F_o$-F_c map surrounding Cmpd 1 in chain A. Map displayed at **σ**=1.5. **b**, Location of Cmpd 1 binding pocket on MKP5-CD in relation to the catalytic site. Surface representation of MKP5-CD (cyan) in complex with Cmpd 1 (green, space-filling) bound to allosteric site. Cys^{408} is highlighted in yellow. **c**, Key interactions between Cmpd 1 and MKP5-CD, including a hydrogen bond with the backbone of Asn^{448} and **π**-stacking with Tyr^{435}. Other residues involved in hydrophobic interactions also shown. Side chains highlighted in blue. Relevant secondary structure features labeled in purple.

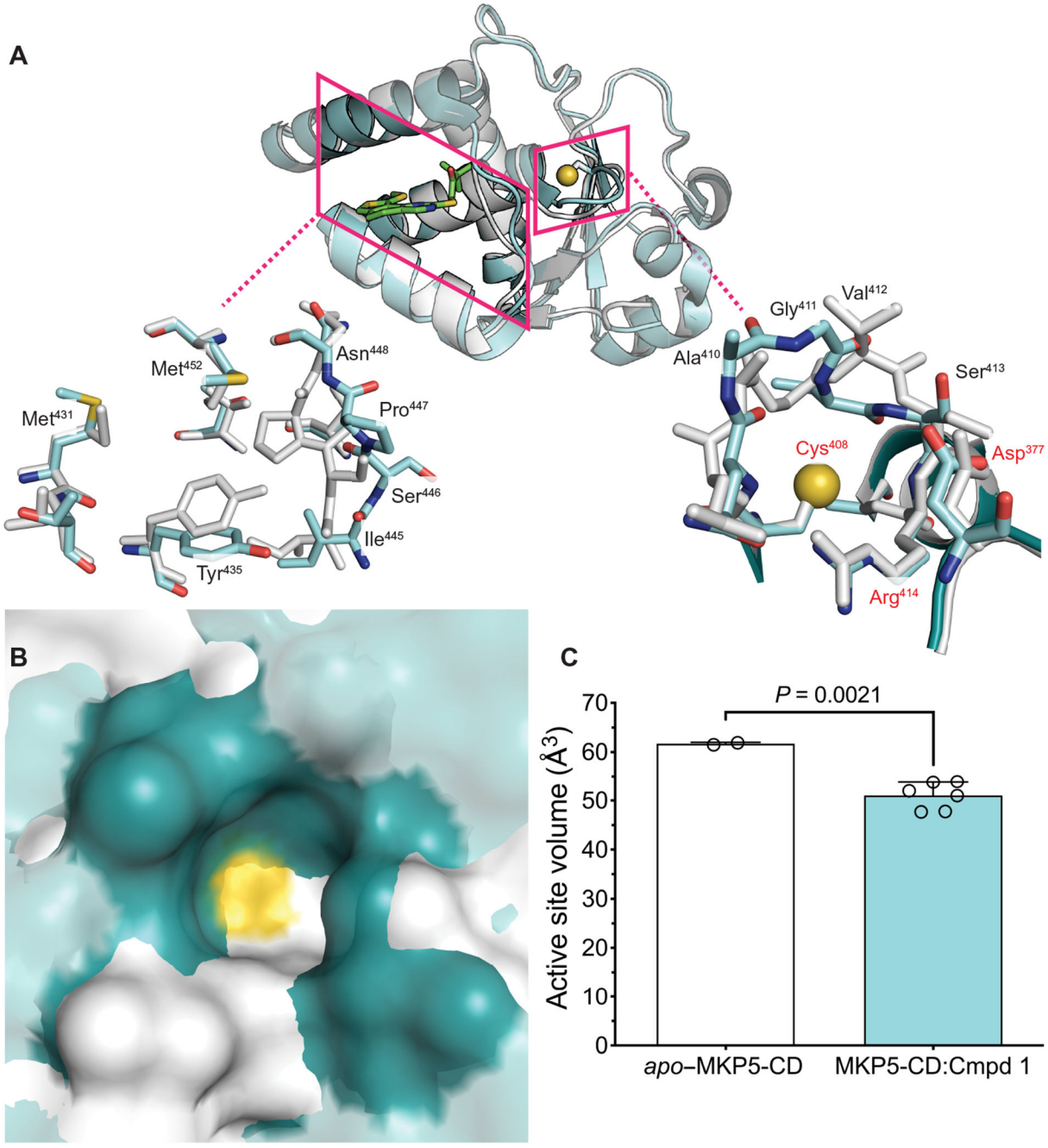

Figure 3. Conformational differences between *apo*- and inhibitor-bound MKP5-CD.

a, Comparison of MKP5-CD:Cmpd 1 (cyan) with *apo*-MKP5-CD (PDB: 1ZZW, white). Full catalytic domains depicted in cartoon representation (top). The allosteric site (bottom left) and catalytic site (bottom right) of MKP5-CD are shown magnified. Residues with large shifts or involved in catalysis are labeled in black and red, respectively. The catalytic sulfhydryl is depicted as a yellow sphere. Cmpd 1 has been removed from the allosteric site zoom for visibility. **b**, Surface representation of the catalytic site of MKP5-CD. Molecules are colored in A. **c**, Quantification of active site volumes in *apo*-MKP5-CD and MKP5-

CD:Cmpd 1 as determined with CAVER Analyst. Data are presented as mean ± SD. Significance determined by two-tailed *t* test ($t = 5.160$, d.f. = 6).

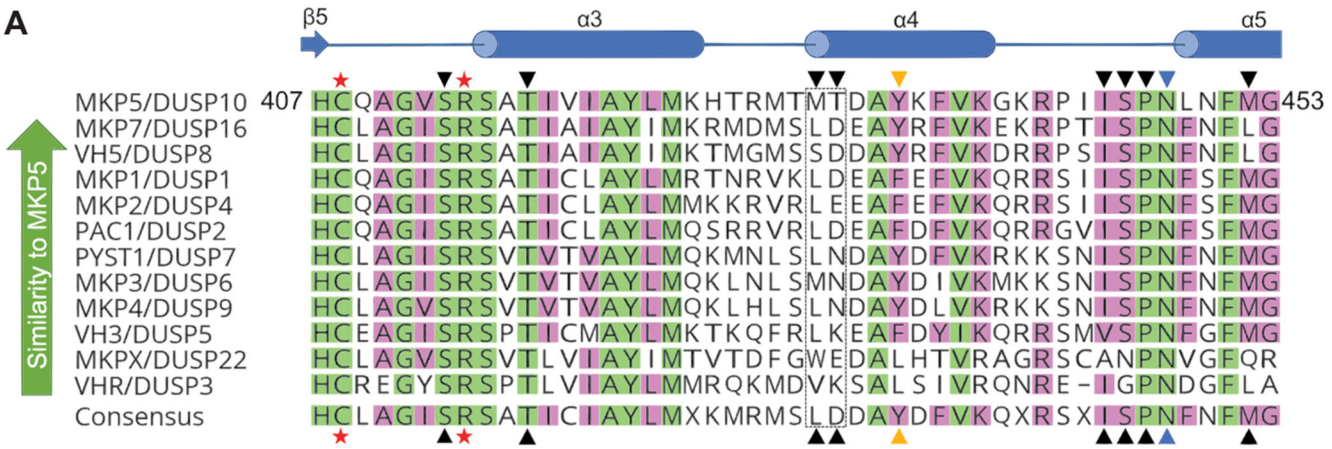

MKP5 construct	K_d (μM)	IC_{50} (μM)
WT	1.0 ± 0.2	3.5 ± 0.5
M431L	22 ± 7	99 ± 12
T432D	>100	61 ± 8
M431L/T432D	>100	>100
Y435A	>100	>100
Y435S	>100	>100
Y435W	1.3 ± 0.3	2.9 ± 0.3

Figure 4. Allosteric pocket of MKP5-CD contains residues critical for catalysis and inhibitor binding

a, Multiple sequence alignment of DUSP catalytic domains. Sequences were aligned using Geneious and sorted by similarity to MKP5/DUSP10. Secondary structure elements of MKP5 indicated above the aligned sequence. Residues that are identical through all DUSPs are highlighted in green, whereas those showing 60% similarity or greater (as determined by BLOSUM62 score of 3 or greater) are highlighted in magenta. Catalytically active residues are indicated with red stars and residues forming interactions with Cmpd 1 are indicated with triangles (yellow – **π**-stacking, blue – hydrogen bonding, black – hydrophobic interactions). **b and c**, Activity (b) and inhibitor binding/potency (c) of mutant MKP5 constructs. Activity was measured using *p*NPP-based assay and normalized against wild-type MKP5-CD. Binding affinity and inhibitor potency against p38α MAPK phosphopeptide determined as in Fig. 1, d, e. MKP1-like mutants conferring selectivity are separated from wild-type and Tyr^{435} mutants by the dashed lines. Data presented as mean ± SD and are the product of three independent experiments.

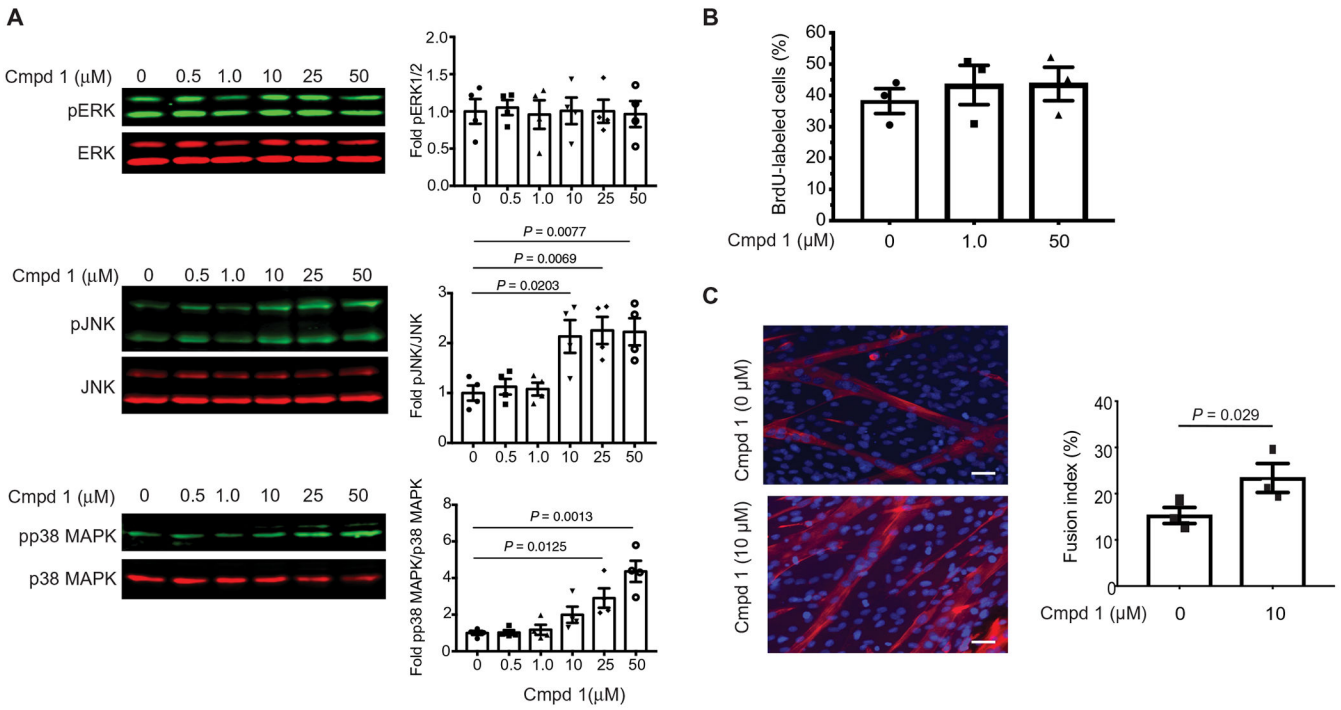

Figure 5. Effect of Compound 1 on MAPK activity

a, Activity of Cmpd 1 on ERK1/2 (upper panel), JNK (middle panel) and p38α MAPK (lower panel) in C2C12 myoblasts. Representative immunoblots of the indicated phosphorylated MAPK (pMAPK) and total MAPK are shown at the left of each graph. Graphs represent the ratio of pMAPK/MAPK as determined by quantitative fluorescent imaging. Data represent means ± SEM of four independent experiments and statistical significance determined by a two-tailed *t*-test is shown. pJNK/JNK; $t = 3.131$, d.f. = 6 (0 versus10 μM); $t = 4.028$, d.f. = 6 (0 versus 25 μM) and $t = 3.931$, d.f. = 6 (0 versus 50 μM). pp38 MAPK/p38 MAPK; $t = 3.518$, d.f. = 6 (0 versus 25 μM) and $t = 5.679$, d.f. = 6 (0 versus 50 μM). **b,** C2C12 myoblasts were cultured in DMSO or Cmpd 1 for 72 hr. Cells were stained with anti-BrdU antibodies and DAPI for nuclei and the percentage of BrdU-positive cells quantitated. Data are derived from three independent experiments and significance was determined by a One-way ANOVA. **c,** C2C12 myoblasts were differentiated for 72 hr in the presence of either DMSO or Cmpd 1, after which cells were stained with MF20 antibody (red) to detect myosin heavy chain and DAPI for nuclei (blue). Representative immunofluorescence images. Scale bar, 100 μM. Differentiation is quantified as a function of myoblast fusion index. Data are derived from three independent experiments and significance was determined by a two-tailed *t*-test (t=5.721, d.f. = 2).

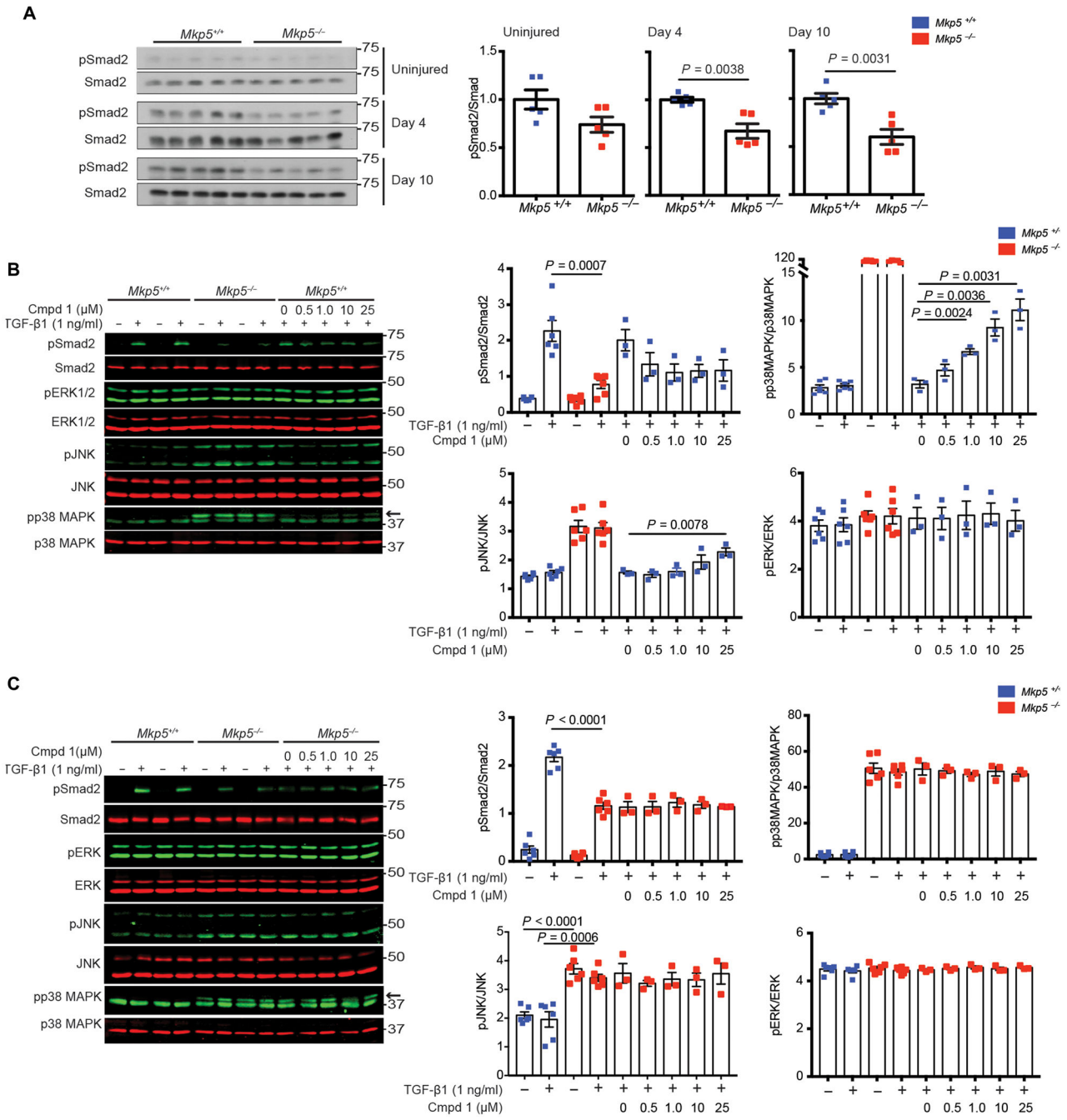

Figure 6. Effect of MKP5 and Compound 1 on TGF-β1-mediated signaling

a, Gastrocnemius muscle from either uninjured or injured *Mkp5*$^{+/+}$ and *Mkp5*$^{-/-}$ mice at 4 and 10 days after cardiotoxin-induced injury were harvested and lysates immunoblotted for pSmad2 and Smad2. Each lane represents results of an animal of the indicated genotype. Graphs represent quantitation of pSmad2 and Smad2 shown as a ratio. Data are means ± SEM and n=5 mice per genotype. **b,** MEFs derived from *Mkp5*$^{+/+}$ and *Mkp5*$^{-/-}$ mice were treated with TGF-β1 (1 ng/ml) for 10 minutes or MEFs from *Mkp5*$^{+/+}$ mice were treated with Cmpd 1 followed by 10 minutes TGF-β1 (1 ng/ml) stimulation. **c**, MEFs derived from

Mkp5$^{+/+}$ and *Mkp5*$^{-/-}$ mice were treated with TGF-β1 (1 ng/ml) for 10 minutes or MEFs from *Mkp5*$^{-/-}$ mice were treated with Cmpd 1 followed by 10 minutes TGF-β1 (1 ng/ml) stimulation. **b, c** Corresponding graphs represent the ratio of pSmad2/Smad2 and pMAPK/MAPK as indicated. Representative immunoblots for the indicated antibodies are shown. Data represent the means ± SEM from 3-6 independent experiments. Statistical significances were determined by *t*-test **a**, pSmad2/Smad2; $t = 4.067$, d.f. = 8 (Day 4) and $t = 4.174$, d.f. = 8 (Day 10). **b**, pSmad2/Smad2; $t = 4.784$, d.f. = 10; pp38α MAPK/p38α MAPK; $t = 6.857$, d.f. = 4 (0 versus 1.0 μM), $t = 6.128$, d.f. = 4 (0 versus. 10 μM); $t = 6.397$, d.f. = 4 (0 versus 25 μM); pJNK/JNK; $t = 4.943$, d.f. = 4 (0 versus 25 μM). **c,** pSmad2/Smad2; $t = 8.651$, d.f. = 10.

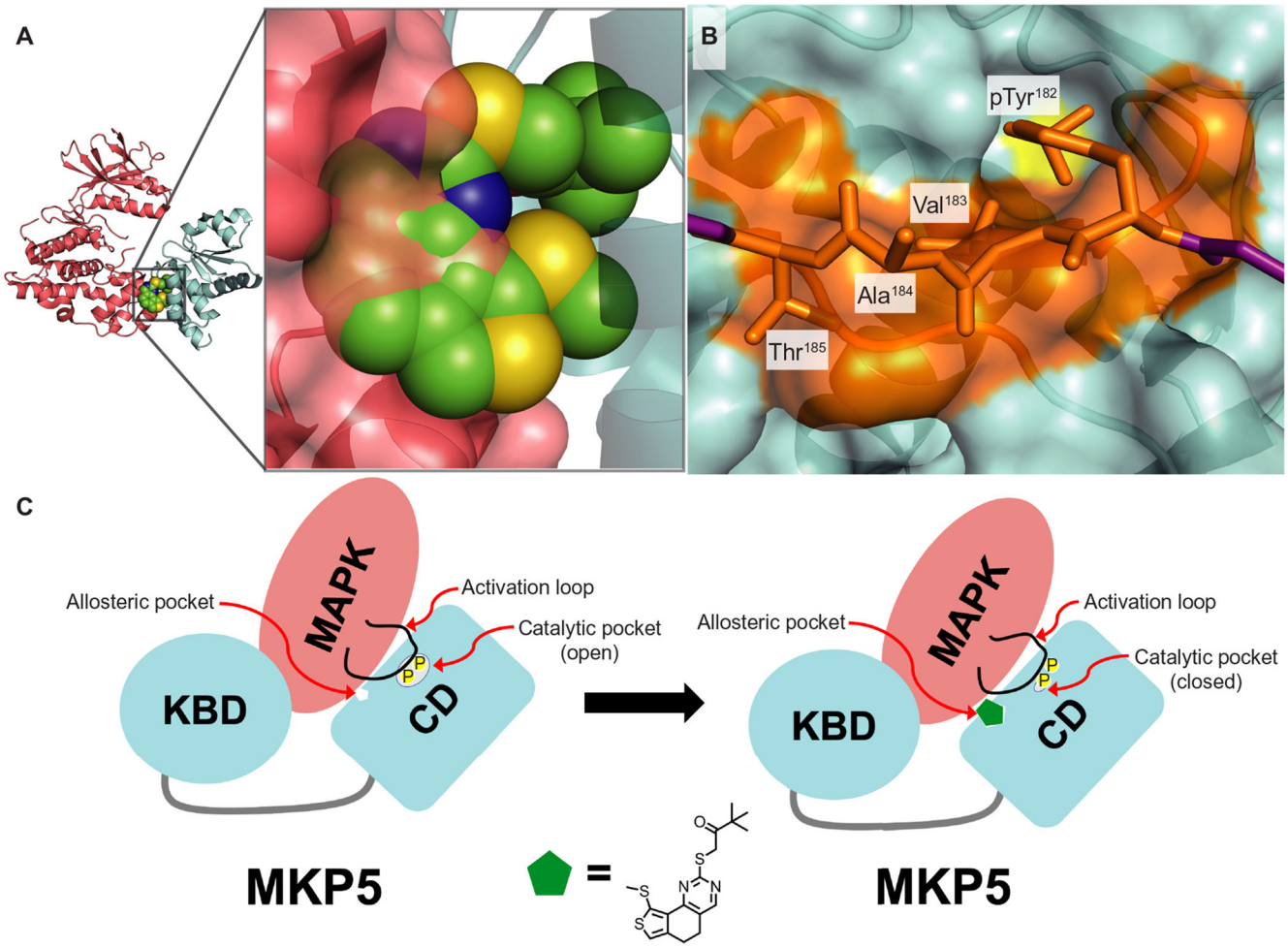

Figure 7. Model for MKP5 inhibition by Compound 1.

a, JNK1 (pink, surface and ribbon) clashes with Cmpd 1 (green, space-filling) bound to MKP5-CD (cyan, ribbon). **b**, Activation loop phosphopeptide (purple) clashes with α4-α5 and β5-α3 loops in MKP5-CD (cyan, surface and ribbon). The catalytic Cys^{408} of MKP5-CD clashes with the activation loop phosphopeptide and is highlighted in yellow, whereas other clashing residues from both MKP5-CD and the phosphopeptide are highlighted in orange. Labeled residues are numbered for corresponding residues in p38α MAPK. Models were generated using PyMOL.align. **c,** MKP5-CD (cyan) in complex with substrate MAPK (pink). The MKP5 catalytic site binds the phosphorylated MAPK activation loop (phosphate - yellow) whereas the allosteric pocket interacts with the αG helix in the MAPK. Cmpd 1 (green) binds at the allosteric site, disrupting both the activation loop and MAPK binding in addition to causing a partial collapse of the active site.